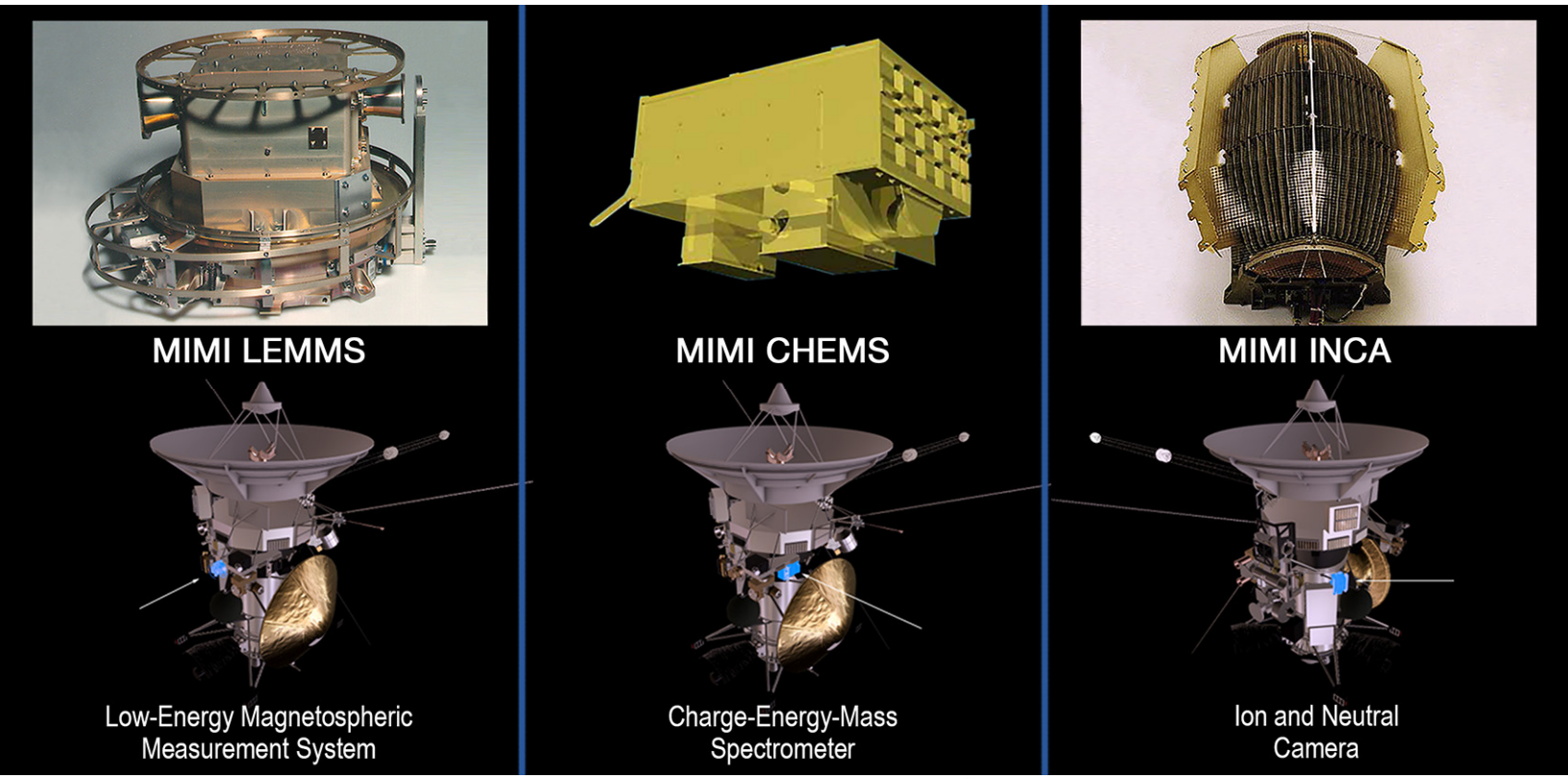

Magnetosphere Imaging Instrument

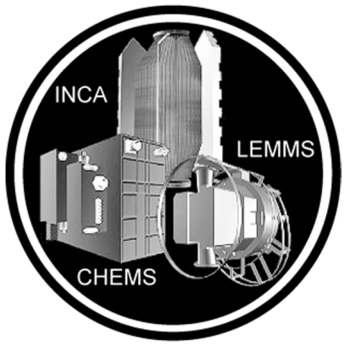

The Magnetosphere Imaging Instrument (MIMI) was comprised of three sensors designed to measure energetic electrons, ions, and neutrals in the Saturn system: the Low Energy Magnetospheric Measurement System (LEMMS), the Charge-Energy-Mass Spectrometer (CHEMS), and the Ion and Neutral Camera (INCA). Each sensor made in situ particle measurements and INCA had the additional capability of creating images out of energetic neutral atoms (ENAs) that can reach the spacecraft from large distances. The **science objectives** of MIMI were to map the charged particle populations of Saturn's magnetosphere, study the global configuration and dynamics of Saturn's magnetosphere and its interaction with the solar wind, Saturn's atmosphere, Titan, and the icy satellites. In concert, MIMI's three sensors extensively characterized the planetary radiation belts of Saturn, discovered a transient radiation belt, and characterized magnetospheric dynamics with global ENA images of Saturn's magnetosphere.

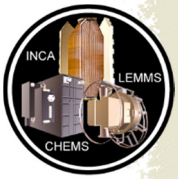

CONTENTS

MAGNETOSPHERE IMAGING INSTRUMENT 1
Executive Summary 3
Instrument Summary 4
Key Objectives for MIMI (Announcement of Opportunity (AO) first, then Cassini Solstice Mission (CSM)) 4
MIMI Science Assessment 5
MIMI Saturn Results 6
Magnetospheric Structure (Roussos) 6
Magnetospheric Dynamics (Paranicas) 10
Periodicities, Solar Cycle, and Seasonal Effects (Carbary) 11
Particle Interactions with Moons and Ring Arcs (Krupp) 12
Space Weathering, Surface Interactions, and Charging (Krupp and Paranicas) 15
Titan (Regoli) 16
The Final Year (Kollmann) 19
Grand Finale Orbits (Paranicas, Kollmann) 20
MIMI Non-Saturn Results 21
Cruise Observations (Carbary) 21
Planetary Flybys (Carbary) 22
Jupiter Cassini-Galileo Comparisons (Krupp) 22
Interplanetary Suprathermal and Energetic Particles (Hill) 24
The Heliosphere Imaged with INCA (Dialynas) 25
Acronyms 29
References 31

Figures

Figure MIMI-1. Flux depletions around Methone's orbit in the LEMMS E4–E6 channels as a function of dipole L shell. 13
Figure MIMI-2. Microsignatures in the LEMMS data. 14
Figure MIMI-3. Microsignature displacements that led to the discovery of a global noon-to-midnight electric field at Saturn. 15
Figure MIMI-4. Sequence of INCA ion images at the highest time resolution available for the ion conic event. 21
Figure MIMI-5. ENA image of the Europa torus. 22
Figure MIMI-6. Differential fluxes and pitch angle distributions of ions and electrons. 23
Figure MIMI-7. A conceptual model of the global heliosphere. 28

Tables

Table MIMI-1. MIMI Science Assessment. 6

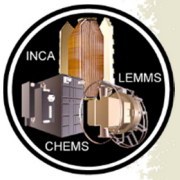

Executive Summary

MIMI measured energetic electrons, ions, and neutrals using three separate sensors: 1) LEMMS, 2) CHEMS, and 3) INCA. Each of these sensors detected particles in the local environment of the spacecraft and INCA had the additional capability of creating images out of ENAs that can reach the spacecraft from large distances. The sensors were able to carry out some separation by species and CHEMS could also separate ions by charge state. MIMI made measurements in cruise and around the planetary flybys and, at Saturn, was operated essentially continuously from orbit insertion in 2004 to the end of mission in 2017. MIMI data characterized Saturn's ion and electron radiation belts; the space environments of the rings, inner satellites, and Titan; and the magnetosphere, high latitude regions, and boundaries, and made advances in our understanding of the dynamics of Saturn's magnetosphere. Through ENA imaging, MIMI also expanded our understanding of the heliosphere.

MIMI extensively characterized the planetary radiation belts of Saturn, including the segmentation of the belts due to the rings and moons and discovered a transient belt.

Highlights from MIMI science. MIMI extensively characterized the planetary radiation belts of Saturn, including the segmentation of the belts due to the rings and moons and discovered a transient belt. INCA obtained global ENA images of Saturn's magnetosphere showing detailed dynamics such as injections, planetary rotational periodicities in ring current intensity, images of the heliosphere and its structure, images of ion acceleration in the auroral region, global ENA emissions of Jupiter, and images of Titan's interaction with the magnetosphere. Satellite and ring absorption signatures predicted a global electric field with no known source. CHEMS and LEMMS data were used to infer regions dominated by the neutral gas torus. MIMI LEMMS measured the inner radiation belts between the middle of the D-ring and the planetary atmosphere. MIMI INCA and CHEMS data led to the discovery of ring dust precipitating into the equatorial atmosphere. MIMI data found periodic features in the magnetosphere.

Key open questions. Some of the open questions relevant to this science are (this follows and expands on the ones in the individual sections below):

- What is the relationship between small and large-scale injections at Saturn and what is the role of injections in the flow of mass and energy through the system?
- What are the mechanisms that create the injections, both in the outer magnetosphere (Titan's orbit and beyond) and between ~18 R_S and Enceladus?
- How do periodicities in charged particle fluxes come about?
- How is the radiation belt inward of the C-ring formed and sustained?

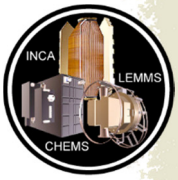

- How can we explain the fluxes of the MeV particles, both inward and outward of the rings and how does the radiation belt co-existing with the F-ring form? What is the source rate of cosmic ray albedo neutron decay (CRAND) neutrons?
- To what extent are the accessible satellite surfaces and atmospheres (including Titan) modified by charged particles?
- What influence does the solar wind have on the magnetosphere?
- Is the mass loss rate from the rings to the atmosphere episodic, or continuous?
- What would Saturn's magnetosphere look like without Enceladus?

Instrument Summary

MIMI comprised three separate sensors and is described in complete detail in Krimigis et al. [2004]. MIMI/LEMMS was a two-ended telescope with oppositely directed fields of view (low and high energy). Detected electrons and ions that entered the apertures were collimated and then reached a solid-state detector (SSD) stack. The stack used a series of coincidence and anti-coincidence requirements related to the energy deposited in the detectors within a timing window to separate species and energies. Electrons entering the low-energy end were magnetically deflected onto detectors for which direct ion pathways are much less probable. Up until about March 2005, a stepping motor changed the telescope fields of view so that good local pitch-angle sampling could be achieved. MIMI/INCA was like a pin-hole camera used to detect ions and ENAs. Collimator blades in front of the detection system could be used to significantly reduce the local charged environment that enters the aperture so that ENAs can be detected more cleanly. When the collimator blade voltages were off, INCA detected the local environment of energetic ions, which typically dominates the neutral intensities. Both ions and neutrals were then measured in a time-of-flight (TOF) system. Secondary electrons triggered start and stop pulses whose positions also identify the particle trajectory. The system was capable of a crude light/heavy ion separation. MIMI/CHEMS measured ions in three directions using an electrostatic analyzer (ESA) followed by a TOF and SSD system. CHEMS stepped through E/q ESA values from about 3 keV/q to 220 keV/q, and selected ions then passed through the TOF system and into one of three SSDs. This allowed for good species and charge state separation (the only sensor on MIMI that can measure charge state). Because of the duty cycle inherent in stepping through 32 E/q steps, CHEMS required more time integration to get good signal statistics.

Key Objectives for MIMI (Announcement of Opportunity (AO) first, then Cassini Solstice Mission (CSM))

- R_AO5 – Ring Magnetosphere-Ionosphere Interactions. Study interactions between the rings and Saturn's magnetosphere, ionosphere, and atmosphere.
- M_AO2 – Magnetosphere Charged Particles. Determine current systems, composition, sources, and sinks of magnetosphere charged particles.

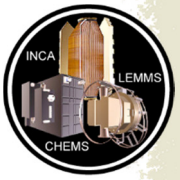

- M_AO4 – Magnetosphere and Solar Interactions with Titan. Study the effect of Titan's interaction with the solar wind and magnetospheric plasma.
- M_AO5 – Plasma Interactions with Titan's Atmosphere and Ionosphere. Investigate interactions of Titan's atmosphere and exosphere with the surrounding plasma.
- I_AO2 – Icy Satellite Surface and Crustal Modifications. Define the mechanisms of crustal and surface modifications, both external and internal.
- I_AO5 – Icy Satellite Magnetosphere and Ring Interactions. Investigate interactions with the magnetosphere and ring systems and possible gas injections into the magnetosphere.
- J_AO3 – Explore the dusk side of the magnetosphere and intermediate regions of the magnetotail unvisited by previous spacecraft.
- C_AO2 – Investigate the behavior of the solar wind during solar minimum, for comparison with earlier Galileo and Ulysses measurements.
- SC2a – Observe the magnetosphere, ionosphere, and aurora as they change on all time scales—minutes to years—and are affected by seasonal and solar cycle forcing.
- MC1a – Determine the temporal variability of Enceladus' plumes.
- MC1b – Observe Saturn's magnetosphere over a solar cycle, from one solar minimum to the next.
- MC2a – Observe seasonal variation of Titan's ionosphere, from one solstice to the next.
- MN1a – Determine the dynamics of Saturn's magnetotail.
- MN1b – Conduct in situ and remote sensing studies of Saturn's ionosphere and inner radiation belt.
- MN1c – Investigate magnetospheric periodicities, their coupling to the ionosphere, and how the Saturn kilometric radiation (SKR) periods are imposed from close to the planet (3–5 R_S) out to the deep tail.
- MN2a – Determine the coupling between Saturn's rings and ionosphere.
- TC2a – Observe Titan's plasma interaction as it goes from south to north of Saturn's solar-wind-warped magnetodisk from one solstice to the next.

MIMI Science Assessment

Table MIMI-1 shows the MIMI science objectives and assessment.

Table MIMI-1. MIMI Science Assessment. AO and Traceability Matrix (TM) objectives are paired with MIMI science objectives.

Fully/mostly accomplished: Partially accomplished: Not accomplished:

MIMI Science Objectives Characterize the following:	AO and TM Science Objectives	MIMI Science Assessment	Comments if yellow (partially fulfilled)
Magnetospheric structure			
Radiation belts and time variations	MN1b		
Composition, sources, and sinks	M_AO2		
Infer neutral properties	MC1a		
Proximal orbits, D-ring gap	M_AO2		
Middle magnetosphere and tail	MN1a		
High latitude magnetosphere, aurorae	SC2a		
Magnetospheric dynamics			
Dynamic phenomena	SC2a		
Periodicities, solar cycle, seasonal effects			
Periodic phenomena	SC2a, MN1c		
Response to season and solar wind	SC2a, MC1b		
Ring and moon interactions			
Moon-magnetosphere interactions	I_AO2, I_AO5		
Ring-magnetosphere interactions	R_AO5, MN2a		
Titan			
Titan-magnetosphere interactions	M_AO4, M_AO5, MC2a, TC2a		
Non-Saturn results			
Properties of the heliosphere			
Jovian magnetosphere	J_AO3		
Properties of the solar wind	C_AO2		

MIMI Saturn Results

Magnetospheric Structure (Roussos)

The structure of Saturn's magnetosphere is complex, due to its colocation with numerous moons, dense and dusty rings, and active plasma sources. Despite that, it is useful to identify several major regions based on which we can organize the MIMI findings. The regions can be naively divided on the basis of the L-shell (which is the field line distance along the magnetic equator in a dipole representation of the magnetic field):

- Inner magnetosphere, containing the radiation belts (L < 9)
- Middle magnetosphere and plasma/sheet (9 < L < 15)
- Outer magnetosphere and magnetotail (L > 15 out to the magnetopause)
- Upstream of the magnetopause

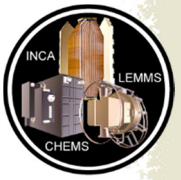

All locations have been extensively sampled by MIMI with different cadence at different mission periods. Below we summarize some of the key results for each region.

Inner magnetosphere and radiation belts: MIMI measurements achieved the most comprehensive description of the radiation belts of a planet besides Earth. More than 200 orbits crossed into the radiation belts, allowing us to understand and quantify their average structure, but also to monitor time variations, despite the single point measurements. The most detailed description of the radiation belts is given by Kollmann et al. [2011] where the L-shell, local time, and pitch angle (latitudinal) structure of the belts is given for electrons and protons of different energies. Heavier ions and their charge states are studied by DiFabio et al. [2011], Dialynas et al. [2009], Carbary et al. [2010a], and Christon et al. [2013, 2014, 2015]. The latter three studies provide the most detailed characterization of trace energetic ions and their charge states at an outer planet, showing how their origin may be connected to the planet's rings, the activity of Enceladus, and seasonal or solar cycle effects.

Allen et al. [2018] conducted a mission-long overview of internal to external sources of energetic plasma at Saturn. They found that solar wind-originating He^{++} ions are able to penetrate into the inner magnetosphere, although the fractional abundance in the inner magnetosphere is only about 0.001%.

Detailed investigations of the proton radiation belts in the MeV range have been published by Roussos et al. [2011, 2016a, 2018a], Kollmann et al. [2013, 2015, 2017], Armstrong et al. [2009], Paranicas et al. [2008, 2010a], and Buratti et al. [2019]. All studies establish how the proton belts are segmented by the icy moons of Saturn (Pandora, Prometheus, Janus, Epimetheus, Mimas, Enceladus, and Tethys) and the planet's main rings. They highlight interaction features with minor rings or ring arcs, such as those from Methone, Pallene, the G-ring, and the ringlets of the D-ring, most of which were unknown prior to Cassini. All studies established that the proton radiation belts inward of Tethys are disconnected from the short-term and large-scale changes that occur in the rest of the magnetosphere, and develop only over long time scales due to the combined influence from variable particle transport effects and the solar cycle, with the former being much more important. The origin of those belts is attributed to CRAND, rather than to extreme solar wind transients, a possibility that was considered before Cassini. Transient extensions of these belts, outside Tethys, have been linked with certainty to the occurrence of interplanetary coronal mass ejections (CMEs) in the vicinity of Saturn [Roussos et al. 2008a, 2018b], one of the first direct demonstrations of space weather at an outer planet with in situ data.

The electron radiation belts in the MeV range have been studied in a series of papers by Roussos et al. [2006, 2014, 2016b, 2019a], Paranicas et al. [2010b, 2012, 2014], Mauk et al. [2010], and Buratti [2019]. They are much more variable and longitudinally asymmetric than the corresponding proton belts, but on average they tend to increase monotonically in intensity inward towards the main rings at which point electrons get instantly absorbed. They evolve in time scales of weeks (as opposed to years for the protons) and are controlled by numerous factors, including the solar wind and internal magnetospheric dynamics. Interaction features of MeV electrons with material—for example, scattering and energy loss in collisions with material—and moons have

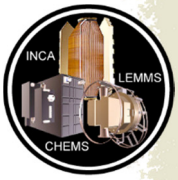

helped to constrain radial transport rates in the magnetosphere and discover previously unknown ring arcs. The source population of the MeV electron belts is now believed to reside in the ring current (middle magnetosphere).

Between energies of tens of keV and few hundred keV, both electrons and ions are on average diminished significantly inward of the orbit of Tethys, due to interactions of these particles with the neutral cloud of Enceladus, the dust of the E-ring or due to absorption by the moons [Paranicas et al. 2007; Kollmann et al. 2011; Carbary et al. 2009a]. The region between 5 and 9 R_S has been found to be dominated by a transient population of interchange injection events, which have been analyzed in single case studies as well as statistically [Paranicas et al. 2007, 2008, 2010b; Mueller et al. 2010; Mauk et al. 2005; and Rymer et al. 2007, 2008, 2009a]. The results have been used to constrain the plasma corotation speed in the inner magnetosphere and the inward radial transport velocities of plasma, and assess the importance of interchange for energetic particle transport and acceleration with respect to other processes like diffusion. The inner magnetosphere is also dominated by energetic electron microsignatures (gaps in the electron fluxes caused by electron absorption by Saturn's moons), which have been used to define the convective flows in the inner magnetosphere (a noon-to-midnight electric field) and radial diffusion rates [Paranicas et al. 2005a; Roussos et al. 2007, 2008a, 2013, 2019a; Andriopoulou et al. 2012, 2014; and Thomsen et al. 2012]. Statistically significant results on the angular distributions and energy spectra of electrons have been described for the first time in Carbary et al. [2011a, 2011b] and Clark et al. [2014].

Middle magnetosphere/ring current: The middle magnetosphere is the region where the so-called ring current of Saturn resides. This current likely has important components below the energy range of MIMI. But it has been found to contain energetic ions and electrons below 1 MeV, with relatively high fluxes. It is populated by large-scale injections in the nightside magnetosphere of Saturn, which sustain the ring current with a series of rotating, energetic ion and electron bundles, sometimes called blobs due to their appearance as such in remote sensing images by MIMI/INCA. The energy density of the energetic ion population is high enough to increase the plasma beta (the ratio of total particle pressure divided by magnetic pressure) above one, therefore causing a significant stretching of the magnetic field lines. Depending on the abundance of oxygen in the energetic ion distributions, the dynamics of the current sheet may be dominated by the presence of energetic particles. All these results are summarized in a series of studies by Sergis et al. [2007, 2009, 2010, 2011, 2013, 2017], Krimigis et al. [2007], Dialynas et al. [2009, 2013a], Carbary et al. [2008a, 2010b, 2012a, 2014a], and Kollmann et al. [2011]. All these measurements provided a most comprehensive, average description of Saturn's ring current, which can inform numerous empirical and physical models of Saturn's magnetosphere—for example, Achilleos et al. [2010]. The time variations in the ring current have been linked to changes in the radiation belts [Roussos et al. 2014, 2018a; Kollmann et al. 2017] and injections [Mitchell et al. 2009a, 2015, 2016], revealing the coupling of the system with different

All these measurements provided a most comprehensive, average description of Saturn's ring current, which can inform numerous empirical and physical models of Saturn's magnetosphere …

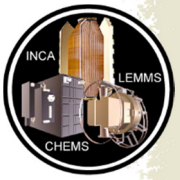

regions of the magnetosphere and the interplanetary space and the aurora—for example, Mitchell et al. [2009b]. The average properties of the ring current, as monitored by ENAs, have been inverted in order to probe the characteristics of Saturn's neutral gas cloud [Dialynas et al. 2013b]. Meanwhile, the average distribution of the middle magnetosphere energetic particles has been studied using observations from CHEMS [Allen et al. 2018].

Many of the studies focusing of the inner magnetosphere extended into the region of the ring current, meaning that energy spectra, angular and L-shell distributions, composition, as well as asymmetries are equally well quantified for $9 < L < 15$.

Outer magnetosphere: Since the outer magnetosphere is very dynamic, it is very challenging to describe its average properties. Still, the continuous in situ measurements by CHEMS and LEMMS and the remote monitoring by INCA have provided unique insights into that region. The most detailed study of the outer magnetosphere's average structure is given by Krimigis et al. [2007] and Sergis et al. [2009], which highlight the distinct day-night asymmetry in the vertical extent of the ring current (or plasma sheet). INCA images have been used to determine the most active sites for dipolarization (or large-scale injection events) in the outer magnetosphere being in the post-midnight sector of the magnetosphere [Mitchell et al. 2005a, 2009b; Carbary et al. 2008b]. They have revealed the wavy structure of the magnetodisk [Carbary 2013; Carbary et al. 2008a, 2015, 2016] and links to auroral emissions. LEMMS measurements have been used to identify an unexpected source of high energy electrons, seen as quasi-periodic pulsations with a period of about 65 minutes. These events are seen globally, they can accelerate electrons to the MeV range instantly and have been linked to reconnection, auroral transients, and similar periodic observations in magnetic field and plasma wave data [Roussos et al. 2016b; Palmaerts et al. 2016a, 2016b; Carbary et al. 2016]. The magnetospheric topology (e.g., open vs. closed field lines or the cusp) has been discussed in the context of MIMI observations—for example, Gurnett et al. [2010] and Arridge et al. [2016a]—while MIMI data have been central in the study and interpretation of reconnection/dipolarization events, in combination with other datasets—for example, Badman et al. [2013, 2016], Jackman et al. [2008, 2015], and Masters et al. [2010]. CHEMS observations also revealed outer magnetosphere asymmetries in the fractional abundance of solar wind-originating ions penetrating into the magnetosphere of Saturn [Allen et al. 2018]. These asymmetries indicate that solar wind He^{++} particles may be entering the magnetosphere due to a combination of Dungey-type reconnection as well as Kelvin-Helmholtz instabilities [Allen et al. 2018].

Upstream of the magnetopause: MIMI measurements have been used to characterize the environment also upstream of the magnetopause. In particular, Sergis et al. [2013] described the conditions of the planet's magnetosheath (the region of shocked solar wind outside the magnetopause), showing how it is strongly modified in the absence or presence of escaping, heavy energetic ions. Kanani et al. [2010] has factored in MIMI measurements to improve empirical models of the shape of Saturn's magnetopause. Measurements of Cassini in the solar wind extend the findings of Sergis et al. [2013], showing the escape of magnetospheric species into interplanetary space [Krimigis et al. 2009a]. Masters et al. [2013] have used MIMI measurements of energetic electrons to demonstrate how the bow shock at very high Mach numbers can be an efficient accelerator of electrons into relativistic energies.

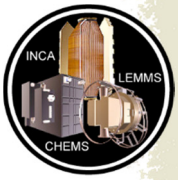

Open questions: What processes form and sustain the newly discovered radiation belt inward of the C-ring? How are energetic particles accelerated at Saturn and how are two-component spectra formed?

Magnetospheric Dynamics (Paranicas)

In addition to the magnetospheric structure presented above, a key aspect of Saturn's magnetosphere is its dynamics. This includes changes on long time scales (months to years) such as the formation and subsequent decay of transient radiation belts [Roussos et al. 2008a] or the gradual evolution of the main radiation belts [Kollmann et al. 2017]. On much shorter time scales, there are both global and more spatially limited injections of hotter plasma or energetic charged particles into the magnetosphere; see Thomsen et al. [2013] for a complete review of the subject. Other dynamics, like pulsations [Palmaerts et al. 2016b] and [Mitchell et al. 2016], are considered in the section entitled Periodicities, Solar Cycle, and Seasonal Effects.

Injections at Saturn have been coarsely characterized as small and large scale. The latter would likely be accompanied by reconfigurations of the planetary magnetic field. Small-scale injections are probably narrow in planetary longitude and physically can be flux tube bundles, flow channels, or more elaborate structures. This group of injections also perturbs the magnetic field locally—for example, Andre et al. [2005, 2007]—but probably at the level of a few percent of the planetary field. Andre et al. [2007] and Rymer et al. [2009a] present multi-instrument displays of interchange events in the magnetosphere of Saturn. This group of injections have been characterized as particle distributions with phase space densities that are very different from the surrounding medium in which they are observed [Mauk et al. 1999; Paranicas et al. 2016]. Mitchell et al. [2015] summarized the observational differences between small-scale and large-scale injections at Saturn. They found that small-scale injections tended to be found inward of about 12–15 R_S, although they also found large-scale injections that could be inward of that distance. It is probably the case that small-scale injections (which are found very frequently in the data) extend in energy up to the tens of keV or so. Rymer et al. [2007] used phase space density profiles derived from Cassini Plasma Spectrometer (CAPS) data to approximate a starting radial distance of interchange injections that are observed by Cassini. Paranicas et al. [2016] approximated the inward flow speed of injections and found values comparable to the theoretical computations of Hill et al. [2016] for $5 < L < 10$. It is believed that the radial speed of injections decreases as they approach Saturn.

Large-scale injections at Saturn have received much less attention in the literature than small-scale ones. Thomsen et al. [2013] have provided a good summary of the situation. Large-scale injections have been characterized by the MIMI data set. Mitchell et al. [2009b] linked some of these injections to ultraviolet (UV) data from Hubble Space Telescope (HST) and Cassini. Paranicas et al. [2007, 2010b] looked at the radial range of injection remnants. Because these extend into the hundreds of keV, it is likely Paranicas was studying large-scale injections. The effects of tail collapse, plasmoid production, and related processes have been documented with the help of magnetometer data—for example, Jackman [2011, 2015].

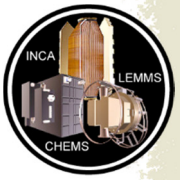

Because of their ubiquity, injections at Saturn have been used to characterize other features of the magnetosphere. Mauk et al. [2005] and Mueller et al. [2010] created azimuthal plasma flow speeds as a function of Saturn distance using MIMI injection data. Plasma flow speeds were later found using the plasma data—for example, Thomsen et al. [2010].

Open questions: What is the connection between large-scale and small-scale injections at Saturn? How much material do injections transport relative to radial diffusion? What creates the injections? How is radial diffusion driven?

Saturn's magnetosphere displays a wealth of periodicities at a wide range of frequency scales.

Periodicities, Solar Cycle, and Seasonal Effects (Carbary)

Saturn's magnetosphere displays a wealth of periodicities at a wide range of frequency scales. The best known of these periodicities is the putative planetary period at ~10.7 hours. This periodicity was discovered in charged particles by the Voyager Low Energy Charged Particle (LECP) instrument in the early 1980s [Carbary and Krimigis 1982]. LEMMS and CHEMS instruments monitored this planetary periodicity throughout the 13-year Cassini mission, and, along with the Radio and Plasma Wave Science (RPWS) and Magnetometer (MAG) instruments, discovered that this periodicity slowly varied by ~1% over several years and that it split into dual periods, one associated with the northern hemisphere and the other with the southern [Carbary et al. 2009b, 2011a]. This dual periodicity is not always detected, however, which may be a consequence of the observer location and/or its actual disappearance [Carbary et al. 2014a, 2016]. Single and dual periodicities were also observed in ENA fluxes detected by INCA [Carbary et al. 2008b, 2014a; Carbary and Mitchell 2017]. INCA's global view of these periodicities revealed a local time dependence, namely, that one period might be detected at one local time but absent at another [Carbary et al. 2014a]. Finally, the energetic electrons apparently have the same period (~10.8 h) during the summer season when either the North or the South Pole tilts with respect to the direction to the Sun [Carbary et al. 2017a]. This discovery, made possible by Cassini's solstice-to-solstice extension, has strong implications for the solar driving of these planetary periodicities. A complete review of Saturn's magnetospheric periodicities, as of 2013, appeared in Reviews of Geophysics [Carbary and Mitchell 2013], and should be consulted for the overall context within which particle periodicities can be placed.

MIMI also discovered that energetic particles display oscillations at the much longer solar wind period (~26 d). This solar wind periodicity was discerned during solar minimum (i.e., 2008–2010) when the solar wind structure was not disrupted by solar activity. The solar wind periodicity was first recognized in the energetic electrons [Carbary et al. 2009c], but was perhaps even stronger in the energetic ions [Carbary et al. 2013a]. Because solar activity varied with the ~22-year solar cycle, the appearance of this 26-day periodicity itself should vary with the solar cycle.

The solar cycle is also evident in LEMMS measurements of Saturn's radiation belts. The very energetic protons (E > 1 MeV) that form Saturn's ionic radiation belts were found to be modulated

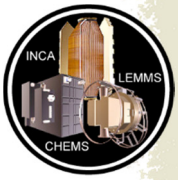

with the solar cycle, which provided clues that they might derive from CRAND from Saturn's atmosphere [Roussos et al. 2011]. As at Earth, the cosmic rays causing CRAND at Saturn are themselves modulated by the solar cycle, and LEMMS detected this for the first time using observations over many years. The ring current boundary, deduced from LEMMS observations, also appears to fluctuate in response to solar energetic particle (SEP) events, which are themselves conditioned according to the solar cycle [Roussos et al. 2014].

The LEMMS instrument also discovered another, completely unexpected periodicity at the relatively short time scale of ~1 hour [Roussos et al. 2016b]. These quasi-periodic (QP) oscillations have periods near ~60 minutes, tend to occur on the dusk side, and suggest acceleration at high latitude [Palmaerts et al. 2016a]. Similar QP-60 oscillations were detected in the polar cusp regions and are probably related to similar periodicities observed in the magnetic field and radio emissions [Palmaerts et al. 2016b]. The ~60-minute periodicities may be related to pulsed dayside reconnection, which generates Alfvén waves having these periods.

Open questions: What is the underlying cause of Saturn's periodicities? How are the observed periodicities related to the actual rotation of Saturn, and does it matter?

Particle Interactions with Moons and Ring Arcs (Krupp)

MIMI studied the environment during 23 Enceladus flybys, 5 Dione flybys, 4(5) Rhea flybys, 1 Tethys flyby, a distant Hyperion flyby, and a distant Mimas flyby.

Simon et al. [2015] summarized the moon magnetosphere interaction and compared Cassini data with hybrid code simulations.

Mimas: Hendrix et al. [2012] analyzed the Mimas UV albedo where the space weather effects caused by the energetic particles in the LEMMS energy range play a major role.

Enceladus: Krupp et al. [2012], Krupp et al. [2018a], and Jones et al. [2006a] studied the particle distributions and absorptions features near Enceladus with ramp-like, spike-like, and dust-related features.

Tethys: Roussos et al. [2005] reported low energy electron microsignature observations by LEMMS in the vicinity of Tethys' L-shell, during the first seven orbits of the Cassini mission. Double microsignatures seen for the first time suggest low radial diffusion coefficients and point to dynamic events in the magnetosphere.

Dione: Kotova et al. [2015] studied the particle distributions using particle tracing in hybrid code simulations and Krupp et al. [2013] summarized the LEMMS measurements near Dione.

Rhea: Jones et al. [2008] reported about particle observations possibly due to orbiting dust near Rhea. In Roussos et al. [2008b], three-dimensional hybrid simulations were performed in the vicinity of Rhea, and Roussos et al. [2012] reviewed the energetic electron environment of Rhea's

magnetospheric interaction. Khurana et al. [2017] identified the distant Alfven wing signature of Rhea several hundred moon radii away.

Hyperion: Nordheim et al. [2014] detected a dropout in energetic electrons observed by LEMMS, indicating that the moon and the spacecraft were magnetically connected when the field-aligned electron population was observed. It was shown that this constitutes a remote detection of a strongly negative (about -200 V) surface potential on Hyperion, consistent with the predicted surface potential in regions near the solar terminator.

Roussos et al. [2005] used LEMMS-displaced microsignature measurements near Tethys to study magnetospheric parameters, including a convective electric field.

Paranicas et al. [2005a] showed some of the earliest evidence of two microsignatures from Enceladus and Tethys in the LEMMS data.

Microsignature analysis from Roussos et al. [2007] revealed a high n dependence in $D_{LL} \sim L^n$ and an increase of its value toward equatorial pitch angles. This supports the idea that electron micro-diffusion refills microsignatures and partly accounts for transporting electrons at low L. It is driven by magnetic field pulsations.

Roussos et al. [2008c] looked at several energetic charged particle microsignatures of two Lagrange moons, Telesto and Helene, measured by the LEMMS instrument and inferred the possibility that the 3 km satellite Methone is responsible for two electron microsignatures detected by Cassini close to this moon's orbit; a previously undetected arc of material exists at Methone's orbit (R/2006 S5) (Figure MIMI-1).

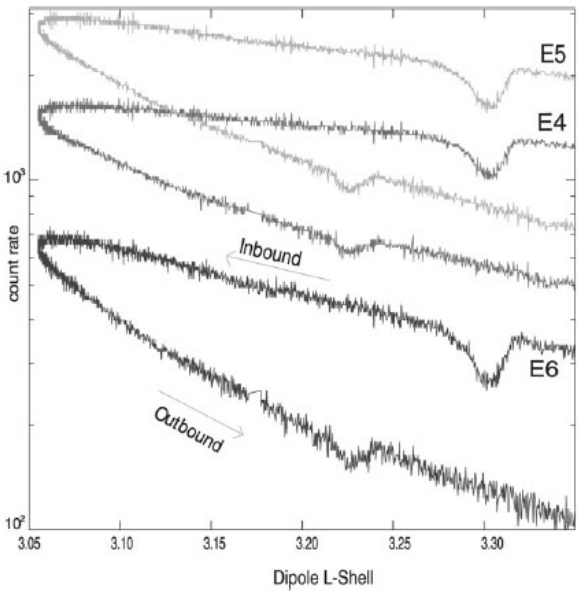

Figure MIMI-1. Flux depletions around Methone's orbit in the LEMMS E4–E6 channels as a function of dipole L shell. [Roussos et al. 2008c]

Roussos et al. [2010a] analyzed energetic electron microsignatures as tracers of radial flows and dynamics in Saturn's innermost magnetosphere including numerical simulation of energetic electron microsignature drifts [Roussos et al. 2013].

Andriopoulou et al. [2012, 2014] discovered a formerly unknown global noon-midnight electric field in Saturn's inner magnetosphere inferred from moon microsignature displacements, by carrying out an analysis of a large amount of LEMMS data (Figure MIMI-2 and Figure MIMI-3).

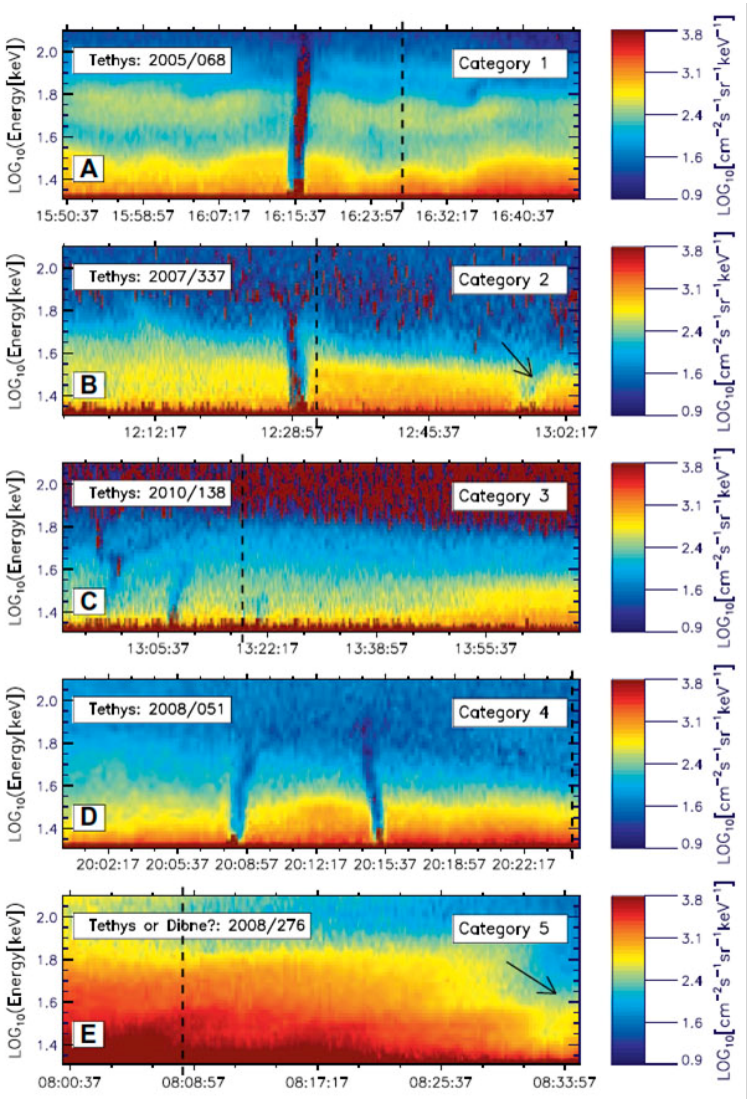

Figure MIMI-2. Microsignatures in the LEMMS data. [Andriopoulou et al. 2012]

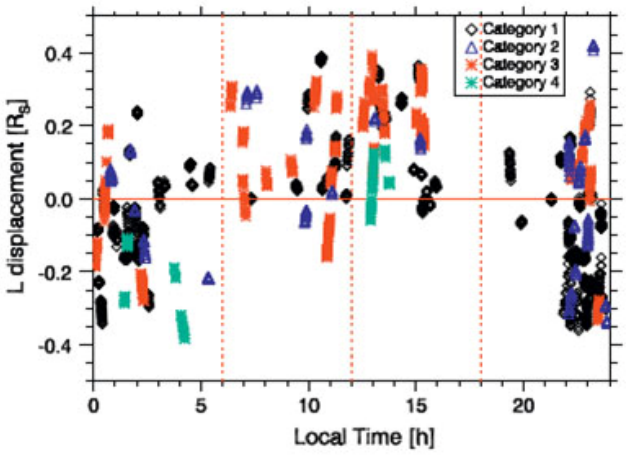

Figure MIMI-3. Microsignature displacements that led to the discovery of a global noon-to-midnight electric field at Saturn. [Andriopoulou et al. 2012]

Some other highlights included a study by Hedman et al. [2007] on the source of Saturn's G-ring and a study by Jones et al. [2006] that found evidence of lightning-induced electron beams in the formation of ring spokes at Saturn.

Open question: What would Saturn's magnetosphere look like without Enceladus?

Space Weathering, Surface Interactions, and Charging (Krupp and Paranicas)

Several optical studies related bombardment patterns by MIMI-range electrons to surface features. Schenk et al. [2011], using a color ratio from Cassini data, found a dark lens shape on the leading hemispheres of Mimas and Tethys that they related to energetic electron bombardment patterns. Howett et al. [2011], using Cassini data from the thermal infrared (IR), predicted that the bombardment of the same energetic electrons could cause regions of thermally anomalous surface ice, meaning the ice would not change temperature in sunlight in a predictable manner. Schiable et al. [2017] expanded on the possible nature of energetic electron bombardment of ice, its effects on spacing in the regolith grains and thermal conductivity.

Paranicas et al. [2014] presented the magnetospheric underpinnings of the lens feature that is observed by Schenk and Howett, following their earlier bombardment model [Paranicas et al. 2001]. Nordheim et al. [2017] expanded on Paranicas's model to include predictions for the bombardment of the leading and trailing hemispheres of Mimas and considered other species in their work.

Paranicas et al. [2018] discussed the energetic proton fluxes at the orbits of the inner moons and argued that the relatively low proton fluxes at the Saturnian moons (compared with the Jovian ones) might be the reason there is little to no amorphous ice in the Saturnian system [Clark et al. 2012]. Buratti et al. [2017] also discussed weathering issues.

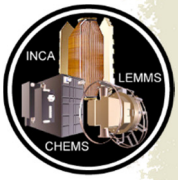

Roussos et al. [2010b] considered the question of the surface charging of Saturn's inner moons.

Open question: Is all the ice in the Saturnian system in the crystalline state and if so why does radiation play no role in causing a transformation to the amorphous state?

Titan (Regoli)

The spacecraft performed 127 flybys of Titan over the course of the whole Cassini mission. The flybys, varying in trajectory and closest approach altitude, served as gravity assists to change Cassini's trajectory, but also to bring our understanding of the moon's environment to an unprecedented level. MIMI's three separate sensors provided a large dataset of the environment surrounding Titan that has already produced important scientific results and that will certainly continue to be analyzed in the decades to come.

The INCA instrument had the capability of remotely measuring the exosphere of Titan, an ambient neutral population too tenuous to be measured by in situ mass spectrometers.

The INCA instrument had the capability of remotely measuring the exosphere of Titan, an ambient neutral population too tenuous to be measured by in situ mass spectrometers. Prior to the arrival of Cassini at Saturn, modeling of the production of ENAs began as a preparation for the first observations. Amsif et al. [1997] developed a model including the inner and outer exosphere, including the five major species contained in Titan's atmosphere, namely, H, H_2, N, N_2, and CH_4. The ENA production was modeled using a proton spectrum from the Voyager flyby. Taking into account the production from both the inner and outer exosphere (estimated using a Chamberlain model), they predicted that Cassini would be able to image the exosphere out to at least 5 Titan radii. Dandouras and Amsif [1999] analyzed the production of synthetic ENA images considering the same exospheric model from Amsif et al. [1997] but including the geometry of the interaction region and the expected ENA trajectories. They concluded that the INCA instrument would be able to provide information regarding the ion fluxes and spectra, as well as the magnetic field environment in the vicinity of Titan, based on a shadowing effect produced by the presence of the moon itself.

Using data from the INCA instrument collected during the first two close flybys of Titan by Cassini, namely TA and TB, Mitchell et al. [2005a] reported a variable halo of ENA emissions that is asymmetric around the moon, confirming the predictions made by the Dandouras and Amsif [1999] model. The overall shape of the ENA images showed a complex interaction region dominated by the variable magnetospheric environment present at the outer magnetosphere and the large gyroradii of the energetic parent ions.

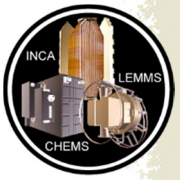

Analyzing the images returned by INCA during the TA flyby, Garnier et al. [2007] found a discrepancy between the maximum flux altitude estimated by the models and the one derived by the data. In order to account for this, they proposed an updated exospheric model, adapted to fit the data provided by the Ion Neutral and Mass Spectrometer (INMS). Using the updated model and energetic ion data obtained by LEMMS, they obtained improved ENA flux profiles that were more consistent with the INCA data.

In a follow-up paper, Garnier et al. [2008] improved the shadowing by the moon by including the corotation velocity of the parent ions. They also found that, to properly interpret INCA data, multiple ionization and neutralization processes for a single parent ion need to be considered. Apart from changing the trajectories, this leads to a thermalization of the energetic ion population.

Combining data from the INCA and the INMS instruments, Dandouras et al. [2009] calculated profiles of the main exospheric species that revealed the non-thermal nature of their distributions. They also found that the ENA emissions from the interaction region get absorbed below an altitude of about 1000 km, where energetic ions deposit their energy. In terms of the extension of the atmosphere, they were able to measure it up to an altitude of 40,000 km.

Using data from Saturn Orbit Insertion (SOI) to 2007, Brandt et al. [2012] studied the exospheric composition of Titan. For this, 36 min accumulation time hydrogen data from the INCA detector when observing Titan without the magnetosphere behind it were analyzed. Combining these observations with a model for the production of ENAs, they found that the molecular hydrogen exosphere of Titan extends to a distance of about 50,000 km—almost 20 Titan radii, confirming the lower-limit of 5 Titan radii obtained by Amsif et al. [1997]. Taking into account the profiles obtained and the fact that ENAs have direct access to Titan's atmosphere, they estimated a precipitating energy flux from ENAs of 5×10^6 keV/(cm^2s), a number comparable to previous estimates of precipitating energetic ions [Sittler et al. 2009] and solar extreme ultraviolet (EUV) [Tobiska 2004].

Apart from remote-sensing studies of the exospheric structure and the interaction region using INCA, CHEMS, and LEMMS also provided in situ data to understand the upstream conditions at Titan's orbit as well as the energy deposition by energetic ions in the atmosphere. Cravens et al. [2008] studied the energy deposition by energetic H^+ and O^+ ions using two different LEMMS spectra: one for the T5 flyby that presented especially high fluxes, and one for a more typical condition. Using a combination of INMS measurements and an engineering model by Yelle et al. [1997] of Titan's atmosphere, they calculated the ionization rates for the precipitating ions concluding that these are important for the formation of the ionospheric layers below the main ionospheric peak as well as for the creation of negative ions observed by the CAPS instrument [Coates et al. 2007].

Smith et al. [2009] focused on the T18 flyby to study the energetic proton penetration in the atmosphere. They used LEMMS to obtain the incoming flux of energetic particles and INCA to analyze the proton penetration at lower altitudes than the Cassini closest approach distance. With these data, they derived an updated atmospheric model that they successfully used to reproduce the INCA observations.

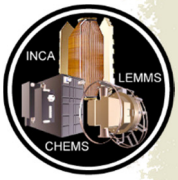

Using a combination of a test particle code and hybrid simulations, Regoli et al. [2016a] analyzed the effect that the magnetic field configuration has on the access and subsequent energy deposition of energetic ions from the Saturnian magnetosphere. Using upstream fluxes detected by CHEMS during the T9 flyby, they found that the ionization rates can vary by up to 80% from one location to another, due to finite gyroradius effects.

From the beginning of the Cassini mission, it became clear that the conditions assumed using the data collected by Voyager in the vicinity of Titan were not representative of the highly variable magnetospheric environment surrounding the moon. The fact that the moon is located at the outskirts of the magnetosphere and that the Saturnian current sheet is constantly moving up and down [Arridge et al. 2008] means that Titan can be located at completely different environments in rapid succession.

Rymer et al. [2009b] used a combination of the electron measurements taken by the Electron Spectrometer (ELS; part of CAPS) and LEMMS instruments to classify the plasma environment at Titan in four different categories, namely plasma sheet, lobe-like, magnetosheath, and bimodal, each with a distinct electron spectrum. They found that the bimodal distribution seems to arise from enhanced local pickup, introducing a cold electron population not present in the other environments. They also found that current sheet encounters were the more common ones, with magnetosheath ones being fairly rare, even though over half of the analyzed encounters occurred within two hours of noon, in terms of Saturn local time.

Using the same technique and instrumentation, Smith and Rymer [2014] extended the study up to the final data sampled by CAPS, before the instrument was switched off in 2012. For that study, they included the remaining dedicated flybys as well as all the orbit crossings when Titan was not there. With this extended dataset (77 encounters and 111 orbit crossings), they derived an empirical model for the electron distribution and also for the rate of occurrence of each environment with respect to Saturn local time.

A similar statistical analysis, but only looking at the energetic ions was made by Garnier et al. [2010] using LEMMS data for ions with energies from 27 to 255 keV and H ENA images corresponding to energies between 24 and 55 keV. They found that the ion population seems to be quasi-isotropic and a dawn-dusk asymmetry in the flux of energetic ions, with higher fluxes in the dawn sector of the magnetosphere. They also concluded that the variability observed in the ENA images from INCA are due to the variability in the magnetospheric fluxes, with the exosphere being roughly stable.

Bebesi et al. [2012] analyzed the locations of the mass-loading boundary (defined as the region where corotating plasma starts to slow down) and the electron drop-out region (where energetic electrons strongly interact with the moon’s atmosphere). They found that the location of these regions presents a scattering that they attributed to the highly variable magnetospheric environment.

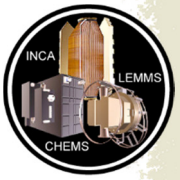

Roussos et al. [2018c] took advantage of the ability of SEPs to penetrate the magnetospheric boundaries to use LEMMS as an upstream monitor to detect solar events even when Cassini is located inside the Saturnian magnetosphere. By performing a statistical study, they identified times with enhanced energetic protons, some of them occurring during dedicated Titan flybys, opening up the possibility of studying the effect that these events have on the energy deposition of energetic particles in the moon's atmosphere.

Using LEMMS and CHEMS data, Regoli et al. [2018] analyzed the energetic environment at the orbit of Titan from a statistical perspective, also finding a highly variable environment, but with a relatively clear distinction for the times when Titan is located inside and outside the Saturnian current sheet. In addition, using Kappa distribution functions, they derived an empirical model of the energetic protons that the moon encounters while orbiting Saturn.

Open questions: How do changes in the energetic environment affect the ionization of Titan's atmosphere? How does the induced magnetosphere of Titan react to changes in the solar wind when Titan is located beyond the Saturnian bow shock?

The Final Year (Kollmann)

The last year of the Cassini mission facilitated a variety of unique measurement opportunities that were not possible throughout the entire previous mission. This began in November 2016 with the so-called F-ring or ring-grazing orbits. Cassini not only came close to the edge of the main rings, it also kept revisiting this region every week. This allowed studying the time dependence of energetic charged particles in this region. Roussos et al. [2018d] reported on a strong enhancement of >1 MeV electrons inward of 6 R_S, possibly due to acceleration in the magnetotail. The fast sequence of orbits allowed observing the time evolution of the enhancement. It is consistent with radial diffusion driven by fluctuations of the noon-to-midnight electric field. Electrons that are quasi stationary in local time (because magnetic and corotation drifts cancel out) are affected the most. Their transport and subsequent loss is much faster than for the stably trapped protons in the same region.

In April 2017, the proximal orbits began, also called the mission Grand Finale. This enabled a comprehensive study of the proton radiation belt trapped approximately between the F-ring and A-ring. MIMI also found a previously unknown partial, electron belt within the F-ring (called "microbelt")—partial because it is only observed outbound at local noon. This microbelt is variable in intensity, although permanently present and stable in local time and L-shell. These results are compiled in Buratti et al. [2019] and Roussos et al. [2019a]. As part of the latter study, it was also shown that a small flux of particles observed on field lines above Saturn's main rings, are actually secondary MeV electrons that were produced by galactic cosmic ray (GCR) impacts on ring material, less than 1 sec before their observation. A clear radial profile of the rings, including the signature of the Cassini division, was visible on the MeV electron rates from LEMMS. This signal has been observed in the past by Pioneer 11 measurements, but it was unclear if those secondary electrons were from GCR impacts on the atmosphere or the rings.

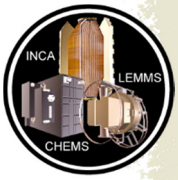

The LEMMS instrument discovered a previously unknown radiation belt collocated with the D-ring and extending up to the dense atmosphere of Saturn. This belt was predicted earlier [Kollmann et al. 2015] but its properties were unknown. It was found that the belt is dominated by protons up to the GeV range, which is the first time that such high energies were directly observed at any of the giant planets. The suggested source is CRAND because protons are unable to diffuse past Saturn's dense A–C rings. There is no evidence for the presence of energetic electrons or ions heavier than protons. These results are compiled in Roussos et al. [2018d]. A follow-up study by Kollmann et al. [2018a] studied the pitch angle distribution and explained its steepness with a strong interaction with Saturn's atmosphere and D-ring. Particle fluxes inward of the main rings can therefore be diagnostic of properties of the D-ring and high-altitude exosphere that are difficult to constrain by other Cassini instruments or remote observations. During SOI, Cassini remotely detected protons at tens of kiloelectron volt (keV) from low (atmospheric) altitudes [Krimigis et al. 2005]. The proximal orbits revealed that this was a huge coincidence since similar observations were only found once during the proximal orbits [Krupp et al. 2018b], suggesting this ion population is transient. Since the ions derive from ENAs produced in the magnetosphere, their intensity likely depends on the conditions in the magnetosphere. Because these ions were not observed in situ, they must be located at altitudes below 3,800 km.

The most surprising measurement during the proximal orbits was likely that the MIMI/INCA and CHEMS instruments, which were designed to measure energetic particles, were detecting signatures of D-ring dust falling into Saturn's equatorial atmosphere. These particles are of 1–3 nm size, much smaller than what is detected by the Cosmic Dust Analyzer (CDA) instrument designed to measure dust. The dust is reaching the atmosphere within 4 h and provides a continuous influx of about 5 kg/s from the rings into the atmosphere. These results are compiled in Mitchell et al. [2018].

Open questions: How can we explain the fluxes of the MeV particles, both inward and outward of the rings and how does the radiation belt co-existing with the F-ring form? What is the source rate of CRAND neutrons?

Grand Finale Orbits (Paranicas, Kollmann)

Other research articles that significantly included MIMI data from the Grand Finale orbits are described next. Mitchell et al. [2018] participated in a series of articles about D-ring dust falling into the planet. They looked at signatures of this process in two of the MIMI sensors and found evidence for grain sizes that cannot be measured by the dedicated dust instrument CDA on Cassini. The spiraling dust may be an explanation for Saturn's hydrogen plume [Shemansky et al. 2009]. Roussos et al. [2018b] described heliospheric conditions inferred from MIMI data obtained at Saturn. Buratti et al. [2019] showed the relationship between trapped charged particles and the locations of small bodies close to the planet.

MIMI Non-Saturn Results

Cruise Observations (Carbary)

Ion conics were observed in proximity to a shock structure in the solar wind between the orbits of Jupiter and Saturn. These conics appear in energetic protons (~30–350 keV) detected by INCA during its approach to Saturn on October 8, 2003 (d 281) and again on October 20, 2003 (d 293).

Both conics have a distinct ring structure centered approximately on the magnetic field, but the first one was peaked along the field at ~35° pitch angles while the second peaked near ~145° anti-parallel to the field. Figure MIMI-4 shows these rings at several energies. The conics lasted for about an hour and display a time and energy dependence. Such events are seen rarely during the Cassini transit between Jupiter and Saturn, even when the spacecraft pointing was favorable near a shock. The conic structures can be explained as a consequence of back-scattering from a nearby shock in the solar wind [Decker et al. 1988]. These results were described by Hill et al. [2006].

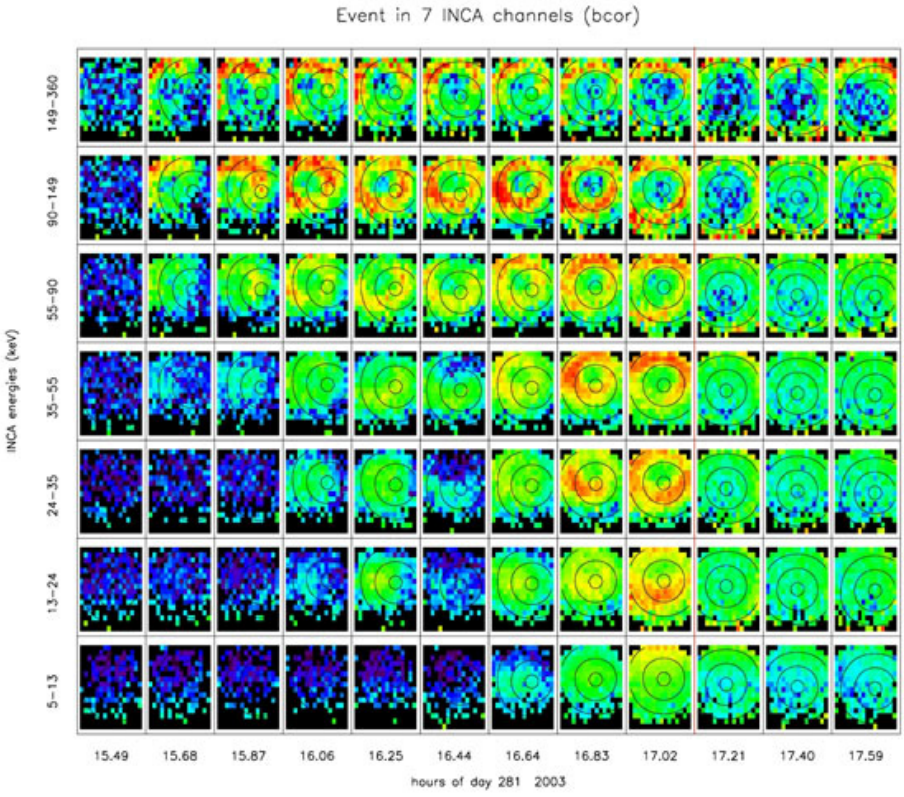

Figure MIMI-4. Sequence of INCA ion images at the highest time resolution available for the ion conic event. With pitch angles contours shown at increments of 10°, 30°, 50°, the images are arranged with time on the horizontal axis and INCA energy on the vertical. Images have been corrected for background and the solar wind flow. The vertical red line between 17.02 h and 17.21 h marks the time of the forward shock. The intensity scales in all cases are logarithmic, although they have different low- and high-energy limits.

Planetary Flybys (Carbary)

The Cassini spacecraft obtained gravity-assists at Earth (August 1999) and Jupiter (December 2000–January 2001). During the Earth flyby, MIMI operated for the first time in a planetary magnetosphere. INCA observed Earth's ring current from long range, CHEMS detected H^+ and O^+ from the outer ring current, and LEMMS reported complete energy spectra of ions and electrons during the pass, including bow shock and magnetopause crossings [Krimigis et al. 2004; Lagg et al. 2001; Ogasawara et al. 2011]. During the Jupiter flyby, INCA observed large fluxes of energetic neutral atoms, primarily H and O, from the planet [Mitchell et al. 2004]. INCA discovered an ENA torus associated with and located just outside the orbit of Europa [Mauk et al. 2003]. The neutral densities in this torus were comparable to those found in the Io-associated cloud, and suggested that Europa is a strong source of neutrals. Figure MIMI-5 shows the discovery ENA image of the Europa torus.

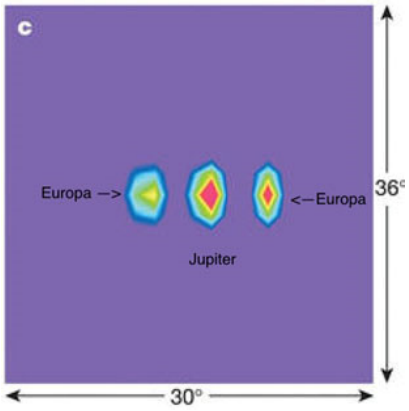

Figure MIMI-5. ENA image of the Europa torus. Seen from the side during the Cassini flyby of Jupiter in early 2001, the Europa torus appears on either side of Jupiter. The image was deconvolved for point sources and corrected for background. The intensity scale is linear.

Jupiter Cassini-Galileo Comparisons (Krupp)

During the Jupiter flyby of Cassini at the end of 2000/beginning of 2001, the Galileo spacecraft was still orbiting the gas giant. The LEMMS sensor was flown on both missions with nearly the same capabilities and identical energy channel configurations. This offered the opportunity to study the duskside Jovian magnetosphere from two different locations simultaneously. The comparison of both energetic particle measurements is summarized in Krupp et al. [2002, 2004].

Figure MIMI-6 shows the differential fluxes and the pitch angle distributions of ions and electrons measured with LEMMS onboard Galileo and Cassini in the vicinity of the Jovian magnetopause. The main results are:

- Passage of closed to open planetary field lines with distributions from bidirectional to monodirectional, with respect to the magnetic field near the magnetopause;
- Periodic variations of electron fluxes on both spacecraft with 40 min periods near Cassini and about 60 min at Galileo's location;

- Leakage of magnetospheric particles into the interplanetary space; and
- Sporadic electron beams outside the magnetosphere (Cassini at 300–900 R_J and Galileo at 130 R_J).

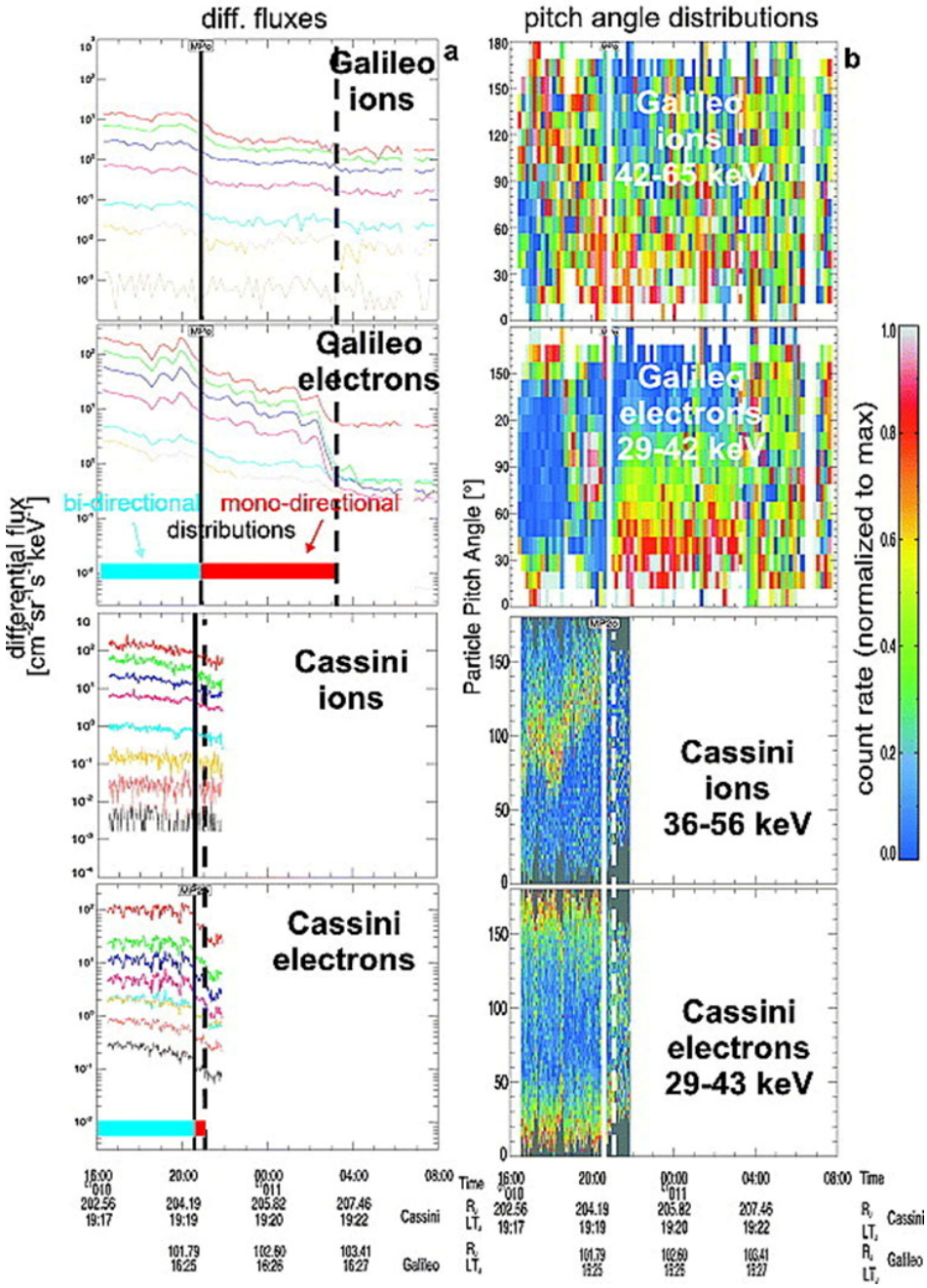

Figure MIMI-6. Differential fluxes and pitch angle distributions of ions and electrons. These ions and electrons are measured with the LEMMS sensors onboard Galileo and Cassini [Krupp et al. 2002] in the vicinity of the magnetopause of Jupiter.

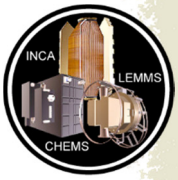

Hanlon et al. [2004] also studied dual spacecraft observations near Jupiter. Cassini data were used as upstream monitors while Galileo was deep inside the Jovian magnetosphere.

Interplanetary Suprathermal and Energetic Particles (Hill)

During the cruise to Saturn, the MIMI suite was able to make unique measurements of heliospheric suprathermal particles in the 2–60 keV/nuc range. There has never been an investigation with species separation of this important class of particles, which ties the solar wind plasma to the energetic particles, beyond Jupiter. Hill et al. [2009] made CHEMS measurements that revealed that the radial intensity profiles of He^{+} and He^{++} are very different from both analytical and numerical theory, with the observations showing an increasing intensity with distance from the Sun, while the theory predicts the intensity should fall. This observation remains unexplained.

CHEMS measurements of pickup ions were used to determine solar wind speeds, which enabled a study [Hill and Hamilton 2010] of the spectral index of suprathermal particles. The slopes of the spectra were reported and widely put into and used to create context by the community, but Hill and Hamilton [2010] showed that the expected velocity v dependence was approximately v-5 as reported by Fisk and Gloeckler [2008]. This study was followed up by Kollmann et al. [2019]. They compared Cassini and New Horizons measurements of interplanetary suprathermal ions. This revealed that there is no obvious dependence of the average spectral shape with distance to the Sun but that that the variability at Cassini's location was much larger. They also suggested a mechanism through which the suprathermal ions are accelerated. The data are consistent with acceleration happening largely in corotating interaction regions. Particles leaving these regions and flowing along magnetic field lines are cooled, so that their spectral shape is changing with distance to the emission region.

The solar wind speeds that were derived with CHEMS data are of inherent value for investigating the heliosphere and, near Saturn, as an input to magnetospheric studies. Data from 2001 to 2004, inclusive, at a 12-hour cadence, were published on the Cassini project's MAPSview website in 2014 (mapskp.cesr.fr/index.php).

The energetic particle population was studied by Lario et al. [2004] using LEMMS observations. They found that intensity enhancements up to ~1 MeV were due to the passage of interplanetary shocks while at the highest energy (>25 MeV), the prompt component of solar energetic particle events was responsible. For all but the largest SEP events, the presence of magnetic field structures between the Sun and the spacecraft significantly modulates the intensity enhancements.

Furthermore, the extension of LEMMS's capabilities to monitor galactic cosmic rays, was used to disprove a theory and Earth-based observations that Jupiter contributes up to 5% of the 80 MeV-2.5 GeV proton flux in the heliosphere [Roussos et al. 2019b].

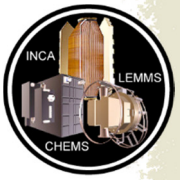

The Heliosphere Imaged with INCA (Dialynas)

The Sun's atmosphere is not static, but expands in the form of a magnetized fluid called the solar wind [Parker 1958], reaching to distances of potentially hundreds of astronomical units (1 AU = 1.5 × 108 km), shaping our local bubble, called the heliosphere, through its interaction with the Local Interstellar Medium (LISM). Voyager 1 and Voyager 2 (hereafter, V1 and V2) crossed the termination shock, where the supersonic solar wind presumably terminates at the shock front, at respective distances of ~94 and ~84 AU in 2004 and 2007 at +35° and −26° ecliptic latitudes [Decker et al. 2005, 2008], pinpointing both the—previously unanticipated—size of the local heliosphere and the scale of the heliospheric asymmetry.

After the discovery of the reservoir of ions and electrons that constitute the heliosheath (a region past the termination shock), V1 passed through an unexpected depletion region, where a decrease in ions of solar origin (by a factor of ~103) and a simultaneous increase of high-energy cosmic rays (~9.3%) occurred, that forms part of the interface between the solar plasma and the galaxy, namely the heliopause [Krimigis et al. 2013], at a distance of ~122 AU. Since August 2012, V1 has continued its journey to the galaxy, measuring the distant and unexplored LISM (V1 is currently located at a distance of ~19 AU past the heliopause), while V2 is still surveying the heliosheath (expected to cross the heliopause in the next few years). Due to the powerful synergy between in situ ions from V1/Low Energy Charged Particle (LECP) instrument and ENAs from INCA (in overlapping energy bands), MIMI, beginning in about 2009, has made key discoveries that altered our past notions on the formation and interactions of the heliosphere, leading to a number of surprises concerning the physics that governs this enormous system, and providing insights on the plasma processes at ~100 AU that were substantially at variance with previous theories and models.

In 2009, the MIMI team published one of the most historic papers, of worldwide appeal, in the field of Heliosphere Physics in Science [Krimigis et al. 2009b]. They showed, for the first time, images of the global heliosphere using >5.2 keV ENA measurements obtained with INCA over the 2003–2009 time period, and identified two striking, previously unexpected, heliospheric signatures: (a) the Belt, a broad band of emission in the sky, identified as a high intensity, relatively wide ENA region that wraps around the celestial sphere in ecliptic coordinates, passing through the nose the anti-nose (tail) and the North and South Heliosphere poles; and (b) the Basins, identified as two extended heliosphere lobes where the ENA minima occur. Interestingly, the ENA measurements are moderately well organized in galactic coordinates, with the Belt presenting a prominent tilt of ~30° with respect to the galactic equator, whereas the Basins were found to roughly coincide with the galactic North and South Poles, although their boundaries were also tilted ~30° to the galactic equator. The same *Science* issue hosted yet another significant publication (with contribution from the then-MIMI PI, S. M. Krimigis), from the Interstellar Boundary Explorer team [McComas et al. 2009], showing, for the first time, images of the heliosphere in <6 keV ENAs. A narrow bright ENA stripe known as the ribbon forms an incomplete circle around the heliospheric nose, most prominent at ~1.1 keV, surrounded by a broad ENA emission that became known as Globally Distributed Flux (GDF).

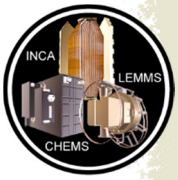

In a later publication, Dialynas et al. [2013a] found that the deviation of the ENA emissions from the equator is effectively minimized in a rotated frame—interpreted as interstellar magnetic field frame (ISMF)—where its North Pole points toward 190° ecliptic longitude and 15° ecliptic latitude. The ENA spectra showed a power-law form in energy, presenting higher spectral slopes in the belt region and lower outside ($3.4 < \gamma < 4.4$), which are almost indistinguishable between the tail and the nose regions, i.e., no noticeable asymmetry was observed. Notably, the morphology of the belt (peak, width, and structure) is nearly energy independent of energy from 5.2 keV to 30 keV. The authors speculated that Interstellar Boundary Explorer (IBEX)-GDF evolves with increasing ENA energy to form the belt at high GDF energies, explaining that the GDF and the ribbon are distinct features that originate from different source plasma populations (heliosheath and outside the heliopause, respectively). This was recently confirmed by the IBEX team [McComas et al. 2017].

Taking into account the local partial pressure over the ~5 < E < 4000 keV energy range from V1, V2, and INCA (~0.1 pPa), an assumed thickness of the heliosheath (~50 AU) and the simulated PUI (pick-up ion) distribution [Giacalone and Decker 2010] that was used to estimate the E < 6 keV contribution (~0.12 pPa), Krimigis et al. [2010] concluded that there is a need for a substantially stronger magnetic field upstream of the heliopause than assumed before, in order to balance the non-thermal PUI pressure against the stagnation pressure of the interstellar plasma and the local ISMF at the heliospheric nose. The interstellar magnetic field was estimated to be ~0.5 nT and have an upper bound of ~0.64 nT. This calculation was confirmed a few years later after V1 crossed the heliopause and measured a strong interstellar magnetic field of ~0.5 nT [Burlaga et al. 2013] that exhibited a jump right outside the heliopause of ~0.6 nT. V1 is currently located at ~19 AU past the heliopause and still measures a magnetic field of ~0.5 nT [Burlaga and Ness 2016], and a relatively dense plasma of >0.09/cm^3 that reached densities of ~0.12/cm^3 [Gurnett et al. 2013, 2015].

A different study, Dialynas et al. [2015] analyzed separately INCA images of the heliosphere and found that the very low (basin) and high (tail) ENA emissions in the heliosheath are separated with a relatively smooth boundary (called transition region), with a spatial width of ~30° in ecliptic longitude, which no theory had predicted to date. The ENA intensity gradient in this transition region was found to be almost invariant as a function of both ecliptic latitude and energy, with an average value of ~2.4% per degree and translates to a corresponding partial pressure gradient that occurs in the transition region, enabling a discussion on the Parker field towards the tail. Bearing in mind that the plasma-β inside the heliosheath showed large fluctuations about an average of ~5–10, i.e., much larger than unity [Decker et al. 2015], this pressure gradient is possibly not consistent with a tail magnetic field configuration that is similar to the measured magnetic fields by the Voyagers in the nose hemisphere. Notably, the pick-up ion populations in the keV range play a dominant role in maintaining the pressure balance in the heliosheath.

In the pre-INCA imaging era, the size of the heliosphere had been estimated using several different models, where the heliosheath varied between 70 and 160 AU. By combining Voyager in situ ion measurements and remotely sensed INCA ENAs in overlapping energy bands, Krimigis et al. [2009b, 2010], calculated that the heliosheath thickness should be ~54 (+30, −15) AU. A more

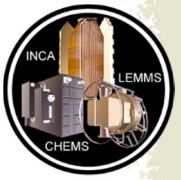

detailed analysis performed by the MIMI team also included the possible contributions from the Compton-Getting effect due to the radial velocity of the heliosheath plasma and concluded that the heliosheath appears to be twice as thick along the V2 line of sight (LOS) as it is along the LOS to V1: L_{V1} = 31 (+31, −18) AU and L_{V2} = 71 (+30, −15) AU [Roelof et al. 2012]. A breakthrough occurred in 2011 when the MIMI and Voyager teams published a brief report [Krimigis et al. 2011] showing that the radial component of the bulk plasma velocity had been decreasing almost linearly for three years, from 70 km/s to 0 km/s, and then stabilized around this value for ~8 months. This study concluded that the ENA and ion spectra could be brought into agreement at V2 with a heliosheath thickness of L_{V2} ~54 (+30, −15) AU, whereas the same normalization procedure applied to Voyager 1 results in L_{V1} ~27 (+26, −11) AU. Surprisingly, the V1 crossing from the heliopause occurred ~1 month later than anticipated by Krimigis et al. [2011] in August 2012 [Krimigis et al. 2013], showing that the heliosheath thickness towards the nose (at V1 direction) is ~29 AU, i.e., much smaller and more compressed than expected in past models.

Admittedly, one of the milestones in the heliosphere research concerns the shape of this enormous system, because it strongly relates to the interpretation of several phenomena that were either theorized in the literature and/or resulted from measurements performed by modern detectors. For more than five decades, the shape and interactions of the heliosphere with the local interstellar medium have been discussed in the context of either a magnetosphere-like heliotail or a more symmetric bubble shape, posited in 1961 [Parker 1961]. Although past models broadly assumed the magnetosphere-like concept, the accurate heliospheric configuration remained largely undetermined due to lack of measurements.

Building upon previous analyses made by Krimigis et al. [2009b] and Dialynas et al. [2013a], and employing both Voyager in situ and INCA remote measurements, a recent MIMI publication, Dialynas et al. [2017a] used >5.2 keV ENA measurements obtained with MIMI/INCA over the 2003–2014 time period and provided a new paradigm on the heliosphere interaction with the LISM: the belt corresponds to a reservoir of particles that exist within the heliosheath, constantly replenished by new particles from the solar wind, while the ENAs that INCA detects are most likely associated with a region of enhanced particle pressure that is formed inside the heliopause and contributes to balancing the pressure of the ISMF. The authors showed that the heliosheath ions are the source of >5.2 keV ENA and that the heliosphere responds promptly, within ~2–3 years, to outward propagating solar wind changes (controlled by solar sunspot numbers and solar wind energy input) in both the upstream (nose) and downstream (tail) directions. These observations, taken together with the V1 measurement of a ~0.5 nT interstellar magnetic field, plasma density of >0.09/cm^3 and the enhanced ratio between particle pressure and magnetic pressure in the heliosheath, strongly suggest a diamagnetic bubble-like heliosphere with few substantial tail-like features. A follow-up MIMI publication [Dialynas et al. 2017b] discussed the details of these results, and by calculating the recovery times of ENAs in the heliosphere, they found that the rough width of the heliosheath can be ~80–120 AU (or more) towards the tail, due to the ~2–3 year delay after solar minimum (Figure MIMI-7).

Dialynas et al. [2017a] also included two important implications concerning the heliosphere interaction with the LISM: 1) A perfectly symmetric and stable heliosphere in time would not be

possible and/or physically correct, i.e., as the heliosphere cannot be a closed system, the heliosphere bubble can (and must) inflate with time in either the anti-nose direction (tail models) or along the direction of the interstellar magnetic field (note that the polar jets [Opher et al. 2015; Drake et al. 2015], provide one of the possible mechanisms through which the solar wind input is evacuated from the system); and 2) due to the strong interstellar magnetic field, the Mach number of the local interstellar medium can be significantly decreased and the flow can become submagnetosonic, leading to the inability of forming a bow shock, as previously explained by Fahr et al. [1986] and simulated from Kivelson and Jia [2013] using the mini magnetosphere of Ganymede as a rough analogy to the heliosphere.

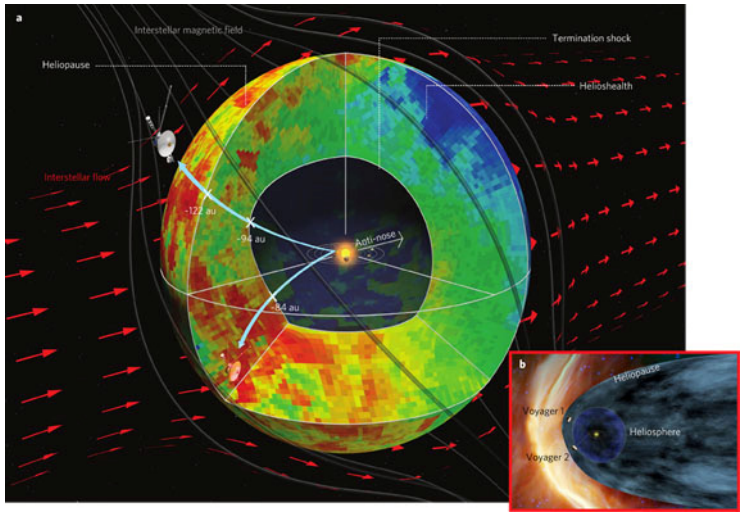

Figure MIMI-7. A conceptual model of the global heliosphere. Adapted from Dialynas et al. [2017b] showing: (a) The gross shape and basic properties of the global heliosphere in three dimensions, summarizing our current understanding, based on both remote ENA and in situ ion measurements from Cassini/INCA and LECP/V1&V2, respectively. It shows a belt of varying ENA intensities surrounding the termination shock and extending to the outer boundary of the heliosphere, called the heliopause, as identified by V1; it is anticipated that the heliopause south of the ecliptic will be crossed by V2 within the next few years. The red arrows represent the interstellar plasma flow deflected around the heliosphere bubble. The termination shock and heliopause are marked at the distances (in AU) observed by the Voyagers from 2004 through 2012 in their traversal of the heliosheath. The cutout illustrates the possible distribution of hot ion plasma in the heliosheath discerned by line-of-sight (LOS) ENA images (E > 5.2 keV); relative scale ranging from 1 (blue) to 12 (red). As the ENA emissions detected by INCA are LOS integrated, the third dimension in this composite, conceptual representation of the global heliosheath (presenting the possible ENA distribution confined between the termination shock and the heliopause) is based on the knowledge of the variation of ion intensities measured at the Voyagers towards the nose hemisphere. These ion intensities are representative of the average ENA intensities along any LOS inside the heliosheath. Note that this concept of the heliosphere does not imply a closed system that cannot change its shape towards the tail to release the solar wind energy input. Inside the termination shock the ion intensities are lower by at least ×100. The orbits of the outer planets are drawn to scale around the Sun. Concept (a) is compared with (b), a magnetosphere-like configuration (http://voyager.jpl.nasa.gov/mission/) widely adopted as one of two possibilities put forward by Parker [1961]. The termination shock is ~10 AU further out in the V1 direction, but the heliosheath (HS) is possibly ~30–50% thicker towards the V2 direction (as detailed in the text), inconsistent with a compressed heliosheath in the Southern Hemisphere. That will be determined when V2 crosses the heliopause (HP), expected in the next few years.

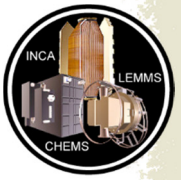

ACRONYMS

Note: For a complete list of Acronyms, refer to Cassini Acronyms – Attachment A.

AU	astronomical unit
CAPS	Cassini Plasma Spectrometer
CDA	cosmic dust analyzer
CHEMS	Charge-Energy-Mass Spectrometer
CRAND	cosmic ray albedo neutron decay
CSM	Cassini Solstice Mission
ELS	Electron Spectrometer
ENA	energetic neutral atom
ESA	electrostatic analyzer
EUV	extreme ultraviolet
e/Q	energy per charge
GCR	galactic cosmic ray
GDF	Globally Distributed Flux
gEV	giga electron volt
HP	heliopause
HS	heliosheath
HST	Hubble Space Telescope
IBEX	Interstellar Boundary Explorer
INCA	Ion and Neutral Camera
INMS	Ion Neutral and Mass Spectrometer
IR	infrared
ISMF	interstellar magnetic field frame
keV	kiloelectron volt
LECP	Low Energy Charged Particle
LEMMS	Low-Energy Magnetospheric Measurement System
LISM	Local Interstellar Medium
LOS	line of sight
MAG	Magnetometer
meV	megaelectron volt
MIMI	Magnetosphere Imaging Instrument
PI	Principal Investigator
PUI	pick-up ion
QP	quasi-periodic
R_J	Jupiter radius
R_S	Saturn radius
RPWS	Radio and Plasma Wave Science
SEP	solar energetic particle

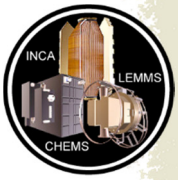

SKR	Saturn Kilometric Radiation
SOI	Saturn Orbit Insertion
SSD	solid-state detector
TM	Traceability Matrix
TOF	time of flight
UV	ultraviolet

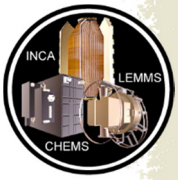

REFERENCES

Disclaimer: The list of references below correspond with in-text references indicated in this report and other articles that rely heavily on MIMI data. For all other Cassini references, refer to Attachment B – References & Bibliographies; Attachment C – Cassini Science Bibliographies; the sections entitled References contributed by individual Cassini instrument and discipline teams located in Volume 1 Sections 3.1 and 3.2 Science Results; and other resources outside of the Cassini Final Mission Report.

Achilleos N., C. S. Arridge, C. Bertucci, P. Guio, N. Romanelli, N. Sergis, (2014), A combined model of pressure variations in Titan's plasma environment, Geophysical Research Letters, 41(24):8730–8735.

Achilleos, N., P. Guio, C. S. Arridge, N. Sergis, R. J. Wilson, M. F. Thomsen, A. J. Coates, (2010), Influence of hot plasma pressure on the global structure of Saturn's magnetodisk, Geophysical Research Letters, 37(L20201).

Allen, R. C., et al. (2018), Internal versus external sources of plasma at Saturn: Overview from MIMI/CHEMS data, Journal of Geophysical Research: Space Physics, 123:4712–4727, doi: 10.1029/2018JA025262.

Amsif, A., J. Dandouras, E. C. Roelof, (1997), Modeling the production and imaging of energetic neutral atoms from Titan's exosphere, Journal of Geophysical Research, 102(22):169–22,181.

André, N., et al., (2008), Identification of Saturn's magnetospheric regions and associated plasma processes: Synopsis of Cassini observations during orbit insertion, Reviews of Geophysics, 46, doi: 10.1029/2007RG000238.

André, N., et al., (2007), Magnetic signatures of plasma-depleted flux tubes in the Saturnian inner magnetosphere, Geophysical Research Letters, 34(L14108).

André, N., et al., (2005), Dynamics of the Saturnian inner magnetosphere: First inferences in the Cassini magnetometers about small-scale plasma transport in the magnetosphere, Geophysical Research Letters, 32(L14SO6).

Andriopoulou, M., E. Roussos, N. Krupp, C. Paranicas, M. Thomsen, S. Krimigis, M. K. Dougherty, K. H. Glassmeier, (2014), Spatial and temporal dependence of the convective electric field in Saturn's inner magnetosphere, Icarus, 229:57–70.

Andriopoulou, M., E. Roussos, N. Krupp, C. Paranicas, M. Thomsen, S. Krimigis, M. K. Dougherty, K. H. Glassmeier, (2012), A noon-to-midnight electric field and nightside dynamics in Saturn's inner magnetosphere, using microsignature observations, Icarus, 220:503–513.

Armstrong, T. P., et al., (2009), Energetic ions trapped in Saturn's inner magnetosphere, Planetary and Space Science, 57(14–15):1723–1731, doi: 10.1016/j.pss.2009.03.008.

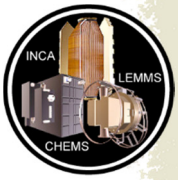

Arridge, C. S., et al., (2016a), Cassini observations of Saturn's southern polar cusp, Journal of Geophysical Research: Space Physics, 121:3006.

Arridge, C. S., et al., (2016b), Cassini in situ observations of long-duration magnetic reconnection in Saturn's magnetotail, Nature Physics, 12:268–271.

Arridge, C. S., M. Kane, N. Sergis, K. K. Khurana, C. M. Jackman, (2015), Sources of local time asymmetries in magnetodiscs, Space Science Reviews, 187:301.

Arridge, C. S., et al., (2011a), Mapping magnetospheric equatorial regions at Saturn from Cassini prime mission observations, Space Science Reviews, 164:1–83.

Arridge, C. S., et al., (2011b), Upstream of Saturn and Titan, Space Science Reviews, 162:25–83.

Arridge, C. S. et al., (2008), Warping of Saturn's magnetospheric and magnetotail current sheets, Journal of Geophysical Research, 113(A8).

Badman, S. V., et al., (2016), Saturn's auroral morphology and field-aligned currents during a solar wind compression, Icarus, 263:83–93.

Badman, S. V., G. Branduardi-Raymont, M. Galand, S. L. G. Hess, N. Krupp, L. Lamy, H. Melin, C. Tao, (2015), Auroral processes at the giant planets: Energy deposition, emission mechanisms, morphology, and spectra, Space Science Reviews, 187(1–4):99–179, doi: 10.1007/s11214-014-0042-x.

Badman, S. V., et al., (2013), Bursty magnetic reconnection at Saturn's magnetopause, Geophysical Research Letters, 40:1027.

Badman, S. V., et al., (2012), Cassini observations of ion and electron beams at Saturn and their relationship to infrared auroral arcs, Journal of Geophysical Research, 117(A01211).

Bebesi, Z., et al., (2012), Analysis of energetic electron drop-outs in the upper atmosphere of Titan during flybys in the dayside magnetosphere of Saturn, Icarus, 218:1020–1027.

Bebesi, Z., et al., (2010), Slow mode shock candidate in the Jovian magnetosheath, Planetary and Space Science, 58:807–813.

Bell, J. M., J. Hunter Waite Jr., J. H. Westlake, S. W. Bougher, A. J. Ridley, R. Perryman, K. Mandt, (2014), Developing a self-consistent description of Titan's upper atmosphere without hydrodynamic escape, Journal of Geophysical Research Space Physics, 119:4957.

Bertucci, C., D. C. Hamilton, W. S. Kurth, G. Hospodarsky, D. G. Mitchell, M. K. Dougherty, (2015), Titan's interaction with the supersonic solar wind, Geophysical Research Letters, 42:193–200.

Beth, A., P. Garnier, D. Toublanc, C. Mazelle, A. Kotova, (2014), Modeling the satellite particle populations in planetary exospheres: Application to Earth, Titan, and Mars, Icarus, 227:21–36.

Blanc, M., D. J. Andrews, A. J. Coates, D. C. Hamilton, C. M. Jackman, X. Jia, A. Kotova, M. Morooka, H. T. Smith, J. H. Westlake, (2015), Saturn plasma sources and associated

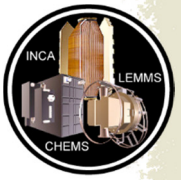

transport processes, Space Science Reviews, 192(1–4):237–283, doi: 10.1007/s11214-015-01792-9.

Blanc, M., et al., (2002), Magnetospheric and plasma science with Cassini-Huygens, Space Science Reviews, 104(1).

Brandt, P. C., K. Dialynas, I. Dandouras, D. G. Mitchell, P. Garnier, S. M. Krimigis, (2012), The distribution of Titan's high altitude (out to ~50,000 km) exosphere from energetic neutral atom (ENA) measurements by Cassini/INCA, Planetary and Space Science, 60:107–114.

Brandt, P. C., et al., (2010), Saturn's periodic magnetic field perturbations caused by a rotating partial ring current, Geophysical Research Letters, 37(L22103), doi: 10.1029/2010GL045285.

Brandt, P. C., C. P. Paranicas, J. F. Carbary, D. G. Mitchell, B. H. Mauk, S. M. Krimigis, (2008), Understanding the global evolution of Saturn's ring current, Geophysical Research Letters, 35(L17101), doi: 10.1029/2008GL034969.

Bunce, E. J., S. W. H. Cowley, D. M. Wright, A. J. Coates, M. K. Dougherty, N. Krupp, W. S. Kurth, A. M. Rymer, (2005), In situ observations of a solar wind compression-induced hot plasma injection in Saturn's tail, Geophysical Research Letters, 32(L20S04), doi: 10.1029/2005GL022888.

Buratti, B. J., et al., (2019), Close Cassini flybys of Saturn's ring moons Pan, Daphnis, Atlas, Pandora, and Epimetheus, Science, 364(6445):eaat2349, doi: 10.1126/science.aat2349.

Buratti, B. J., R. N. Clark, F. Crary, C. J. Hansen, A. R. Hendrix, C. J. A. Howett, J. Lunine, C. Paranicas, (2017), Cold cases: What we don't know about Saturn's moons, Planetary and Space Science, 155:41–49, doi: 10.1016/j.pss.2017.11.017.

Burlaga, L. F., N. F. Ness, (2016), Observations of the interstellar magnetic field in the outer heliosheath: Voyager 1, The Astrophysical Journal, 829:134.

Burlaga, L. F., N. F. Ness, E. C. Stone, (2013), Magnetic field observations as Voyager 1 entered the heliosheath depletion region, Science, 341:147–150.

Carbary, J. F., (2019a), Magnetodisk coordinates for Saturn, Journal of Geophysical Research: Space Physics, 124:451–458.

Carbary, J. F., (2019b), Three dimensional currents in Saturn's magnetosphere, Journal of Geophysical Research: Space Physics, 124:971–981.

Carbary, J. F., D. C. Hamilton, D. G. Mitchell, (2019), Global maps of energetic ions in Saturn's magnetosphere, Journal of Geophysical Research: Space Physics, 123:8557–8571.

Carbary, J. F., (2018), The meridional magnetic field lines of Saturn, Journal of Geophysical Research: Space Physics, 123:6264–6276.

Carbary, J. F., et al., (2018), Energetic electron pitch angle distributions during the Cassini final orbits, Geophysical Research Letters, 45:2911–2917.

Carbary, J. F., (2017), Update on Saturn's energetic electron periodicities, Journal of Geophysical Research: Space Physics, 122:156–165, doi: 10.1002/2016JA023405.

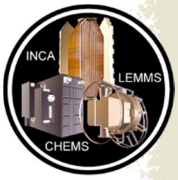

Carbary, J. F., D. G. Mitchell, P. Kollmann, N. Krupp, E. Roussos, (2017a), Energetic electron periodicities during the Cassini grand finale, Journal of Geophysical Research: Space Physics, 122, doi: 10.1002/2017JA024836.

Carbary, J. F., D. G. Mitchell, A. M. Rymer, N. Krupp, D. Hamilton, S. M. Krimigis, S. V. Badman, (2017b), Local time asymmetries in Saturn's magnetosphere, in Dawn-Dusk Asymmetries in Planetary Plasma Environments, (eds.) S. Haaland, A. Runov, C. Forsythm, Geophysical Monograph 230, pp. 323–336.

Carbary, J. F., G. Provan, (2017), Saturn's magnetic field periodicities at high latitudes and the effects of spacecraft motion and position, Journal of Geophysical Research: Space Physics, 122, doi: 10.1002/2016JA023611.

Carbary, J. F., D. G. Mitchell, (2017), Midnight flash model of ENA periodicities at Saturn, Journal of Geophysical Research: Space Physics, 122(7), doi: 10.1002/2017JA024296.

Carbary, J. F., A. M. Rymer, (2017), Solar wind periodicities in thermal electrons at Saturn, Journal of Geophysical Research: Space Physics, 122, doi: 10.1002/2016JA023531.

Carbary, J. F., W. S. Kurth, D. G. Mitchell, (2016), Short periodicities in low-frequency plasma waves at Saturn, Journal of Geophysical Research: Space Physics, 121:6562–6572.

Carbary, J. F., D. G. Mitchell, (2016), Seasonal variations in Saturn's plasma sheet warping, Geophysical Research Letters, 43:11,957–11,962, doi: 10.1002/2016GL071790.

Carbary, J. F., (2016), A new spiral model of Saturn's magnetosphere, Geophysical Research Letters, 43:501–507.

Carbary, J. F., (2015a), A new approach to Saturn's periodicities, Journal of Geophysical Research: Space Physics, 120:6436–6442.

Carbary, J. F., (2015b), Doppler effects on periodicities in Saturn's magnetosphere, Journal of Geophysical Research: Space Physics, 120:9457–9470.

Carbary, J. F., N. Sergis, D. G. Mitchell, N. Krupp, (2015), Saturn's hinge parameter from Cassini magnetotail passes in 2013–2014, Journal of Geophysical Research: Space Physics, 120:4438.

Carbary, J. F., M. Kane, B. H. Mauk, S. M. Krimigis, (2014a), Using the kappa function to investigate hot plasmas in the magnetospheres of the giant planets, Journal of Geophysical Research, 119, doi: 10.1002/2014JA020324.

Carbary, J. F., D. G. Mitchell, P. C. Brandt, (2014b), Local time dependences of oxygen ENA periodicities at Saturn, Journal of Geophysical Research, 119, 2014JA020214.

Carbary, J. F., D. G. Mitchell, (2014), Keogram analysis of ENA images at Saturn, Journal of Geophysical Research, 119, doi: 10.1002/2014JA019784.

Carbary, J. F., A. M. Rymer, (2014), Meridional maps of Saturn's thermal electrons, Journal of Geophysical Research: Space Physics, 119, doi: 10.1002/2013JA019436.

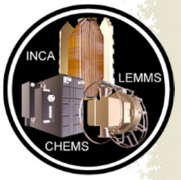

Carbary, J. F., (2013), Wavy magnetodisk in Saturn's outer magnetosphere, Geophysical Research Letters, 40:5024.

Carbary, J. F., D. G. Mitchell, (2013), Periodicities in Saturn's magnetosphere, Reviews of Geophysics, 51:1–30.

Carbary, J. F., E. C. Roelof, D. G. Mitchell, D. C. Hamilton, (2013a), Solar periodicity in energetic ions at Saturn, Journal of Geophysical Research, 118, doi: 10.1002/jgra.50282.

Carbary, J. F., et al., (2013b), Longitude dependences of Saturn's ultraviolet aurora, Geophysical Research Letters, 40, doi: 10.1002/grl.50430.

Carbary, J. F., (2012), The morphology of Saturn's ultraviolet aurora, Journal of Geophysical Research, 117(A06210).

Carbary, J. F., N. Achilleos, C. S. Arridge, (2012a), Statistical ring current of Saturn, Journal of Geophysical Research, 117(A06223).

Carbary, J. F., D. G. Mitchell, S. M. Krimigis, N. Krupp, (2012b), Unusually short period in electrons at Saturn, Geophysical Research Letters, 39(L22103).

Carbary, J. F., D. G. Mitchell, S. M. Krimigis, N. Krupp, (2011a), Post-equinox periodicities in Saturn's energetic electrons, Geophysical Research Letters, 28(L24104), 2011GL050259.

Carbary, J. F., et al., (2011b), Energetic electron spectra in Saturn's plasma sheet, Journal of Geophysical Research, 116(A07210).

Carbary, J. F., D. G. Mitchell, P. C. Brandt, S. M. Krimigis, D. A. Gurnett, (2011c), ENA periodicities and their phase relations to SKR emissions at Saturn, Geophysical Research Letters, 38(L16106).

Carbary, J. F., D. G. Mitchell, C. P. Paranicas, E. C. Roelof, S. M. Krimigis, N. Krupp, K. Khurana, M. Dougherty, (2011d), Pitch angle distributions of energetic electrons at Saturn, Journal of Geophysical Research, 116(A01216), doi: 10.1029/2010JA015987.

Carbary, J. F., D. C. Hamilton, S. P. Christon, D. G. Mitchell, S. M. Krimigis, (2010a), Longitude dependencies of energetic H+ and O+ at Saturn, Journal of Geophysical Research, 115(A07226), doi: 10.1029/2009JA015133.

Carbary, J. F., N. Achilleos, C. S. Arridge, K. K. Khurana, M. K. Dougherty, (2010b), Global configuration of Saturn's magnetic field derived from observations, Geophysical Research Letters, 37(L21806), doi: 10.1029/2010GL044622.

Carbary, J. F., D. G. Mitchell, S. M. Krimigis, D. A. Gurnett, W. S. Kurth, (2010c), Phase relations between energetic neutral atom intensities and kilometric radio emissions at Saturn, Journal of Geophysical Research, 115(A01203).

Carbary, J. F., D. G. Mitchell, N. Krupp, S. M. Krimigis, (2009a), L shell distribution of energetic electrons at Saturn, Journal of Geophysical Research, 114(A09210), doi: 10.1029/2009JA014341.

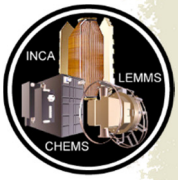

Carbary, J. F., D. G. Mitchell, S. M. Krimigis, N. Krupp, (2009b), Dual periodicities in energetic electrons at Saturn, Geophysical Research Letters, 36(L20103), doi: 10.1029/2009GL040517.

Carbary, J. F., E. C. Roelof, D. G. Mitchell, S. M. Krimigis, N. Krupp, (2009c), Solar wind periodicity in energetic electrons at Saturn, Geophysical Research Letters, 36(L22104), doi: 10.1029/2009GL041086.

Carbary, J. F., S. M. Krimigis, D. G. Mitchell, C. Paranicas, P. Brandt, (2009d), Energetic neutral atom (ENA) and charged particle periodicities in Saturn's magnetosphere, Advances in Space Research, 44:483–493, doi: 10.1016/j.asr.2009.04.019.

Carbary, J. F., D. G. Mitchell, C. Paranicas, E. C. Roelof, S. M. Krimigis, (2008a), Direct observation of warping in the plasma sheet of Saturn, Geophysical Research Letters, 35(L24201), doi: 10.1029/2008GL035970.

Carbary, J. F., D. G. Mitchell, P. Brandt, E. C. Reolof, S. M. Krimigis, (2008b), Track analysis of energetic neutral atom blobs at Saturn, Journal of Geophysical Research, 113(A01209), doi: 10.1029/2007JA012708.

Carbary, J. F., D. G. Mitchell, P. Brandt, C. Paranicas, S. M. Krimigis, (2008c), ENA periodicities at Saturn, Geophysical Research Letters, 35(L07102), doi: 10.1029/2008GL033230.

Carbary, J. F., D. G. Mitchell, P. Brandt, E. C. Roelof, S. M. Krimigis, (2008d), Periodic tilting of Saturn's plasma sheet, Geophysical Research Letters, 35(L24101), doi: 10.1029/2008GL036339.

Carbary, J. F., D. G. Mitchell, P. Brandt, E. C. Reolof, S. M. Krimigis, (2008e), Statistical morphology of ENA emissions at Saturn, Journal of Geophysical Research, 113(A05210), doi: 10.1029/2007JA012873.

Carbary, J. F., D. G. Mitchell, S. M. Krimigis, D. C. Hamilton, N. Krupp, (2007a), Charged particle periodicities in Saturn's outer magnetosphere, Journal of Geophysical Research, 112, 2007JA012351.

Carbary, J. F., D. G. Mitchell, S. M. Krimigis, D. C. Hamilton, N. Krupp, (2007b), Spin-period effects in magnetospheres with no axial tilt, Geophysical Research Letters, 34(L18107), doi: 10.1029/2007GL030483.

Carbary, J. F., D. G. Mitchell, S. M. Krimigis, N. Krupp, (2007c), Evidence for spiral pattern in Saturn's magnetosphere using the new SKR longitudes, Geophysical Research Letters, 34(L13105), doi: 10.1029/2007GL030167.

Carbary, J. F., D. G. Mitchell, S. M. Krimigis, N. Krupp, (2007d), Electron periodicities in Saturn's outer magnetosphere, Journal of Geophysical Research, 112, doi: 10.1029/2006JA012077.

Carbary, J. F., S. M. Krimigis, (1982), Charged particle periodicity in the Saturnian magnetosphere, Geophysical Research Letters, 9:1073–1076.

Carrasco N., J. H. Westlake, P. Pernot, J. H. Waite, Jr., (2013), Nitrogen in Titan's atmospheric aerosol factory, in The Early Evolution of the Atmospheres of Terrestrial Planets, Springer.

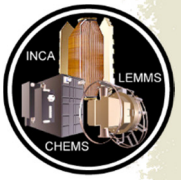

Chen, Y., T. W. Hill, A. M. Rymer, R. J. Wilson, (2010), Rate of radial transport of plasma in Saturn's inner magnetosphere, Journal of Geophysical Research, 115(A10211), doi: 10.1029/2010JA015412.

Christon S. P., D. C. Hamilton, J. M. C. Plane, D. G. Mitchell, J. M. Grebowsky, W. N. Spjeldvik, S. R. Nylund, (2017), Discovery of suprathermal ionospheric origin Fe+ in and near Earth's magnetosphere, Journal of Geophysical Research: Space Physics, 122, doi: 10.1002/2017JA024414.

Christon, S. P., D. C. Hamilton, D. G. Mitchell, R. B. DiFabio, S. M. Krimigis, J. M. C. Plane, (2015), Discovery of suprathermal Fe+ in Saturn's magnetosphere, Journal of Geophysical Research, 120:2720.

Christon, S. P., D. C. Hamilton, D. G. Mitchell, R. B. DiFabio, S. M. Krimigis, (2014), Suprathermal magnetospheric minor ions heavier than water at Saturn: Discovery of 28M+ seasonal variations, Journal of Geophysical Research, 119, 2014JA020010.

Christon, S. P., D. C. Hamilton, R. D. DiFabio, D. G. Mitchell, S. M. Krimigis, D. S. Jontof-Hutter, (2013), Saturn suprathermal O2+ and mass-28+ molecular ions: Long-term seasonal and solar variation, Journal of Geophysical Research, 118, doi: 10.1002/jgra.50383.

Christensen, U., N. Krupp (2009), Die Geschwister der Erde, Physik Journal, 8(5):31–36.

Clark, G., C. Paranicas, D. Santos-Costa, S. Livi, N. Krupp, D. G. Mitchell, E. Roussos, W. L. Tseng, (2014), Evolution of electron pitch angle distributions across Saturn's middle magnetospheric region from MIMI/LEMMS, Planetary and Space Science, 104:18–28, doi: 10.1016/pss.2014.07.004.

Clark, R. N., et al., (2012), The surface composition of Iapetus: Mapping results from Cassini VIMS, Icarus, 218:831–860.

Coates, A. J., et al. (2007), Discovery of heavy negative ions in Titan's ionosphere, Geophysical Research Letters, 34(L22103).

Cooper, J. F., P. D. Cooper, E. C. Sittler, S. J. Sturner, A. M. Rymer, (2009), Old faithful model for radiolytic gas-driven cryovolcanism at Enceladus, Planetary and Space Science, 57:1607–1620.

Crary, F., et al., (2005), Solar wind dynamic pressure and electric field as the main factors controlling Saturn's aurorae, Nature, 433:720–722.

Cravens, T. E., N. Ozak, M. S. Richard, M. E. Campbell, I. P. Robertson, M. Perry, A. M. Rymer, (2011), Electron energetics in the Enceladus torus, Journal of Geophysical Research, 116(A09205).

Cravens, T. E., et al., (2008), Energetic ion precipitation at Titan, Geophysical Research Letters, 35(L03103), doi: 10.1029/2007GL032451.

Dandouras, I., P. Garnier, D. G. Mitchell, E. C. Roelof, P. C. Brandt, N. Krupp, S. M. Krimigis, (2009), Titan's exosphere and its interaction with Saturn's magnetosphere, Philosophical Transactions of the Royal Society, 367, doi: 10.1098/rsta.2008.0249.

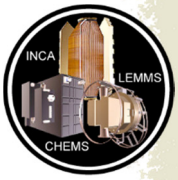

Dandouras, J., A. Amsif, (1999), Production and imaging of energetic neutral atoms from Titan's exosphere: A 3-D model, Planetary and Space Science, 47:1355–1369.

Decker, R. B., S. M. Krimigis, E. C. Roelof, M. E. Hill, (2015), Recent particle measurements from Voyagers 1 and 2, Journal of Physics: Conference Series, 577.

Decker, R. B., S. M. Krimigis, E. C. Roelof, M. E. Hill, T. P. Armstrong, G. Gloeckler, D. C. Hamilton, L. J. Lanzerotti, (2008), Mediation of the solar wind termination shock by non-thermal ions, Nature, 454:67–70.

Decker, R. B., S. M. Krimigis, E. C. Roelof, M. E. Hill, T. P. Armstrong, G. Gloeckler, D. C. Hamilton, L. J. Lanzerotti, (2005), Voyager 1 in the foreshock, termination shock, and heliosheath, Science, 309:2020–2024.

Decker, R. B., (1988), Computer modeling of test particle acceleration at oblique shocks, Space Science Reviews, 48:195–262.

Delamere, P. A., et al., (2015), Solar wind and internally driven dynamics: Influences on magnetodiscs and auroral responses, Space Science Reviews, 187(1–4):51–97, doi: 10.1007/s11213-013-0075-1.

Dessler, A. J., (1985), Differential rotation of the magnetic fields of gaseous planets, Geophysical Research Letters, 12:299–302.

Dialynas, K., et al., (2018), Energetic ion moments and polytropic index in Saturn's magnetosphere using Cassini/MIMI measurements: A simple model based on k-distribution functions, Journal of Geophysical Research: Space Physics, 123, doi: 10.1029/2018JA025820.

Dialynas, K., et al., (2017a), The bubble-like shape of the heliosphere observed by Voyager and Cassini, Nature Astronomy, 1:115.

Dialynas, K., S. M. Krimigis, D. G. Mitchell, R. B. Decker, E. C. Roelof, (2017b), Response times of Cassini/INCA > 5.2 keV ENAs and Voyager ions in the heliosheath over the solar cycle, Journal of Physics: Conference Series, 900(1).

Dialynas, K., C. P. Paranicas, J. F. Carbary, M. Kane, S. M. Krimigis, B. H. Mauk, (2017c), The kappa-shaped particle spectra in planetary magnetospheres, in, Kappa Distributions, Theory and Applications in Plasmas, (ed.) G. Livadiotis, Elsevier, pp. 481–522.

Dialynas, K., S. M. Krimigis, D. G. Mitchell, E. C. Roelof, (2015), Energetic neutral atom (ENA) intensity gradients in the heliotail during year 2003, using Cassini/INCA measurements, Journal of Physics: Conference Series, 577, doi: 10.1088/1742-6596/577/1/012007.

Dialynas, K., S. M. Krimigis, D. G. Mitchell, E. C. Roelof, R. B. Decker, (2013a), A three-coordinate system (Ecliptic, Galactic, ISMF) spectral analysis of heliospheric ENA emissions using Cassini/INCA measurements, The Astrophysics Journal, 778:40.

Dialynas, K., et al., (2013b), The extended Saturnian neutral cloud as revealed by global ENA simulations using Cassini/MIMI measurements, Journal of Geophysical Research, 118:1–15, doi: 10.1002/jgra.50295.

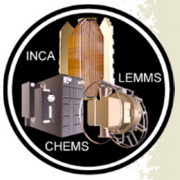

Dialynas, K. S., S. M. Krimigis, D. G. Mitchell, D. C. Hamilton, N. Krupp, P. C. Brandt, (2009), Energetic ion spectral characteristics in the Saturnian magnetosphere using Cassini/MIMI measurements, Journal of Geophysical Research, 114(A01212), doi: 10.1029/2008JA013761.

DiFabio, R. D., D. C. Hamilton, S. M. Krimigis, D. G. Mitchell, (2011), Long term time variations of the suprathermal ions in Saturn's magnetosphere, Geophysical Research Letters, 38(L18103).

Dougherty, M. K., L. W. Esposito, S. M. Krimigis, (2009), Overview, in Saturn from Cassini-Huygens, (eds.) M. K. Dougherty, L. W. Esposito, S. M. Krimigis, Springer, Dordrecht, pp. 1–8.

Drake, J. F., M. Swisdak, M. Opher, (2015), A model of the heliosphere with jets, The Astrophysical Journal Letters, 808, doi: 10.1088/2041-8205/808/2/L44.

Edberg, N. J. T., et al., (2013), Extreme densities in Titan's ionosphere during the T85 magnetosheath encounter, Geophysical Research Letters, 40:1–5, doi: 10.1002/grl.50579.

Fahr, H. J., (1986), Is the heliospheric interface submagnetosonic? Consequences for the LISM presence in the heliosphere, Advances in Space Research, 6:13–25.

Felici, M., et al., (2016), Cassini observations of ionospheric plasma in Saturn's magnetotail lobes, Journal of Geophysical Research: Space Physics, 121:338.

Fisk, L. A., G. Gloeckler, (2008), Acceleration of suprathermal tails in the solar wind, The Astrophysical Journal, 686:1466.

Frisch, P. C., et al., (2010), First global observations of the interstellar interaction from the Interstellar Boundary Explorer (IBEX), Bulletin of the American Astronomical Society, 42:263.

Futaana, Y., J. Chaufray, H. T. Smith, P. Garnier, H. Lichtenegger, M. Delva, H. Groeller, A. Mura, (2011), Exospheres and energetic neutral atoms of Mars, Venus, and Titan, Space Science Reviews, 162:213–266.

Garnier, P., et al., (2012), The detection of energetic electrons with the Cassini Langmuir probe at Saturn, Journal of Geophysical Research, 117(A10202).

Garnier, P., et al., (2010), Statistical analysis of the energetic ion and ENA data for the Titan environment, Planetary and Space Science, 58:1811–1822.

Garnier, P., et al., (2009), Titan's ionosphere in the magnetosheath: Cassini RPWS results during the T32 flyby, Annales Geophysicae, 27:4257–4272.

Garnier, P., et al., (2008), The lower exosphere of Titan: Energetic neutral atom absorption and imaging, Journal of Geophysical Research, 113(A10216), doi: 10.1029/2008JA013029.

Garnier, P., et al., (2007), The exosphere of Titan and its interaction with the kronian magnetosphere: MIMI observations and modeling, Planetary and Space Science, 55:165–173.

Gérard, J. -C., et al., (2006), Saturn's auroral morphology and activity during quiet magnetospheric conditions, Journal of Geophysical Research, 111(A12210), doi: 10.1029/2006JA011965.

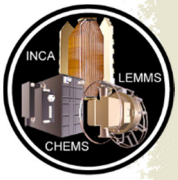

Giacalone, J., R. B. Decker, (2010), The origin of low-energy anomalous cosmic rays at the solar-wind termination shock, The Astrophysical Journal, 710:91–96.

Gombosi, T. I., T. P. Armstrong, C. S. Arridge, K. K. Khurana, S. M. Krimigis, N. Krupp, A. M. Persoon, M. F. Thomsen, (2009), Saturn's magnetospheric configuration, in Saturn from Cassini-Huygens, (eds.) M. K. Dougherty, L. W. Esposito, S. M. Krimigis, Springer, Dordrecht, pp. 203–255.

Gurnett, D. A., W. S. Kurth, E. C. Stone, A. C. Cummings, S. M. Krimigis, R. B. Decker, N. F. Ness, L. F. Burlaga, (2015), Precursors to interstellar shocks of solar origin, The Astrophysical Journal, 809:121.

Gurnett, D. A., W. S. Kurth, L. F. Burlaga, N. F. Ness, (2013), In situ observations of interstellar plasma with Voyager 1, Science, 341:1489–1492.

Gurnett, D. A., et al., (2010), A plasmapause-like density boundary at high latitudes in Saturn's magnetosphere, Geophysical Research Letters, 37(L16806), doi: 10.1029/2010GL044466.

Gurnett, D. A., A. Lecacheux, W. S. Kurth, A. M. Persoon, J. B. Groene, L., Lamy, P. Zarka, J. F. Carbary, (2009), Discovery of a north-south asymmetry in Saturn's radio rotation period, Geophysical Research Letters, 36(L16102), doi: 10.1029/2009GL039621.

Hanlon, P. G., (2004), Dual spacecraft observations of a compression event within the Jovian magnetosphere: Signatures of externally triggered supercorotation, Journal of Geophysical Research, 109(A09S09).

Hedman, M. M., et al., (2007), The source for Saturn's G ring, Science, 317:653–656.

Helled, R., E. Galanti, Y. Kaspi, (2015), Saturn's fast spin determined from its gravitational field and oblateness, Nature, 520:202–204, doi: 10.1038/nature14278.

Hendrix, A. R., G. Filacchione, C. Paranicas, P. Schenk, F. Scipioni, (2018), Icy Saturnian satellites: Disk-integrated UV-IR characteristics and links to exogenic processes, Icarus, 300:103–114.

Hendrix, A. R., et al., (2012), Mimas' far-UV albedo: Spatial variations, Icarus, 220:922–931.

Hill, M. E., D. C. Hamilton, (2010), Interim report on the power law index of interplanetary suprathermal ion spectra, American Institute of Physics Conference Proceedings, 1302:58–63.

Hill, M. E., N. A. Schwadron, D. C. Hamilton, R. D. DiFabio, R. K. Squier, (2009), Interplanetary suprathermal He+ and He++ observations during periods from 1 to 9 AU and implications for particle acceleration, The Astrophysical Journal, 699:L26–L30.

Hill, M. E., C. P. Paranicas, R. B. Decker, D. G. Mitchell, (2006), "Smoke ring" pitch angle distributions of energetic particles associated with shock passage in the middle heliosphere, American Geophysical Union Spring Meeting, Baltimore, MD, May 25, 2006, abstract SH44A-04.

Hill, T., (2016), Penetration of external plasma into a rotation-driven magnetosphere, Journal of Geophysical Research Space Physics, 121:10,032–10,036.

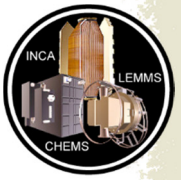

Hill, T. W., et al., (2011), Charged nanograins in the Enceladus plume, Journal of Geophysical Research, 117(A05209).

Hill, T. W., et al., (2008), Plasmoids in Saturn's magnetotail, Journal of Geophysical Research, 113(A01214), doi: 10.1029/2007JA12626.

Howett, C. J. A., A. R. Hendrix, T. A. Nordheim, C. Paranicas, J. R. Spencer, A. J. Verbiscer, (2018), Ring and magnetosphere interactions with satellite surfaces, Enceladus and the icy moons of Saturn, 2(4):343.

Howett, C. J. A., J. R. Spencer, P. Schenk, R. E. Johnson, C. Paranicas, T. A. Hurford, A. Verbiscer, M. Segura, (2011), A high-amplitude thermal inertia anomaly of probable magnetospheric origin on Saturn's moon Mimas, Icarus, 216:221–226.

Jackman, C. M., et al., (2015), Field dipolarization in Saturn's magnetotail with planetward ion flows and energetic particle flow bursts: Evidence of quasi-steady reconnections, Journal of Geophysical Research: Space Physics, 120:3603–3617.

Jackman, C. M., J. A. Slavin, S. W. H. Cowley, (2011), Cassini observations of plasmoid structure and dynamics: Implications for the role of magnetic reconnection in magnetospheric circulation at Saturn, Journal of Geophysical Research, 116(A10212).

Jackman, C. M., et al., (2008), A multi-instrument view of tail reconnection at Saturn, Journal of Geophysical Research, 113(A11), 2008JA013592.

Jasinski, J. M., C. S. Arridge, A. J. Coates, G. H. Jones, N. Sergis, M. F. Thomsen, N. Krupp, (2017), Diamagnetic depression observations at Saturn's magnetospheric cusp by the Cassini spacecraft, Journal of Geophysical Research: Space Physics, 122:6283–6303.

Jasinski, J. M., et al., (2016a), Flux transfer event observation at Saturn's dayside magnetopause by the Cassini spacecraft, Geophysical Research Letters, 43:6713.

Jasinski, J. M., et al., (2016b), Cassini plasma observations of Saturn's magnetospheric cusp, Journal of Geophysical Research: Space Physics, 121.

Jasinski, J. M., et al., (2014), Cusp observation at Saturn's high-latitude magnetosphere by the Cassini spacecraft, Geophysical Research Letters, 41:1382–1388.

Jinks, S. L., et al., (2014), Cassini multi-instrument assessment of Saturn's polar cap boundary, Journal of Geophysical Research, 119:8161–8177.

Johnson, R. E., et al., (2009), Mass loss processes in Titan's upper atmosphere, in Titan from Cassini-Huygens, (eds.) R. H. Brown, J. -P. Lebreton, J. H. White, Springer, Dordrecht, pp. 373–391.

Johnson, R. E., et al., (2008), Sputtering of ice grains and icy satellites in Saturn's inner magnetosphere, Planetary and Space Science, 56, doi: 10.1016/j.pss.2008.04.003.

Jones, G. H., et al., (2008), The dust halo of Saturn's largest icy moon, Rhea, Science, 319:1380–1384.

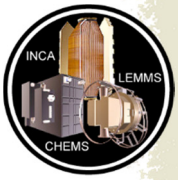

Jones, G. H., et al., (2006a), Enceladus's varying imprint on the magnetosphere of Saturn, Science, 311:1412–1415.

Jones, G. H., et al., (2006b), Formation of Saturn's ring spokes by lightning-induced electron beams, Geophysical Research Letters, 33(L21202), doi: 10.1029/2006GL028146.

Kanani, S. J., et al., (2010), A new form of Saturn's magnetopause using a dynamic pressure balance model, based on in-situ, multi-instrument Cassini measurements, Journal of Geophysical Research, 115(A06207), doi: 10.1029/2009JA014262.

Kane, M., D. G. Mitchell, J. F. Carbary, S. M. Krimigis (2014), Plasma convection in the nightside magnetosphere of Saturn determined from energetic ion anisotropies, Planetary and Space Science, 91(1).

Kane, M., D. G. Mitchell, J. F. Carbary, S. M. Krimigis, F. J. Crary, (2008), Plasma convection in Saturn's outer magnetosphere determined from ions detected by the Cassini INCA experiment, Geophysical Research Letters, 35(L04102), doi: 10.1029/2007GL032342.

Kellett, S., et al., (2011), Saturn's ring current: Local time dependence and temporal variability, Journal of Geophysical Research, 116(A05220).

Kellett, S., et al., (2010), Nature of the ring current in Saturn's dayside magnetosphere, Journal of Geophysical Research, 115(A08201), doi: 10.1029/2009JA015146.

Khurana, K. K., S. Fatemi, J. Lindkvist, E. Roussos, N. Krupp, M. Holmström, C. T. Russell, M. K. Dougherty, (2017), The role of plasma slowdown in the generation of Rhea's Alfvén wings, Journal of Geophysical Research: Space Physics, 122, doi: 10.1002/2016JA023595.

Khurana, K. K., et al., (2009), Sources of rotational signals in Saturn's magnetosphere, Journal of Geophysical Research, 114(A02211), doi: 10.1029/2008JA013312.

Kivelson, M. G., X. J. Jia, (2013), An MHD model of Ganymede's mini-magnetosphere suggests that the heliosphere forms in a sub-Alfvénic flow, Journal of Geophysical Research: Space Physics, 118(11):6839–6846.

Kliore, A. J., A. F. Nagy, T. E. Cravens, M. S. Richard, A. M. Rymer, (2011), Unusual electron density profiles observed by Cassini radio occultations in Titan's ionosphere: Effects of enhanced magnetospheric electron precipitation, Journal of Geophysical Research, 116(A11318).

Kollmann, P., et al., (2019), Suprathermal ions in the outer heliosphere, The Astrophysical Journal, 876:46(10pp), doi: 10.3847/1538-4357/ab125f.

Kollmann, P., et al., (2018a), Saturn's innermost radiation belt throughout and inward of the D ring, Geophysical Research Letters, 45:10,912–10,920, doi: 10.1029/2018GL077954.

Kollmann, P., et al., (2018b), Electron acceleration to MeV energies at Jupiter and Saturn, Journal of Geophysical Research: Space Physics, 123:9110–9129, doi: 10.1029/2018JA025665.

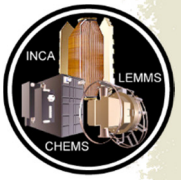

Kollmann, P., E. Roussos, A. Kotova, C. Paranicas, N. Krupp, (2017), The evolution of Saturn's radiation belts modulated by changes in radial diffusion, Nature Astronomy, doi: 10.1038/s41550-017-0287-x.

Kollmann, P., E. Roussos, A. Kotova, J. F. Cooper, D. G. Mitchell, N. Krupp, C. Paranicas, (2015), MeV protons flux predictions near Saturn's D ring, Journal of Geophysical Research Space Physics, 120:8586–8602.

Kollmann, P., E. Roussos, C. Paranicas, N. Krupp, D. K. Haggerty, (2013), Processes forming and sustaining Saturn's proton radiation belts, Icarus, 222:323–341.

Kollmann, P., E. Roussos, C. Paranicas, N. Krupp, C. M. Jackman, E. Kirsch, K. -H. Glassmeier, (2011), Energetic particle phase space densities at Saturn: Cassini observations and interpretations, Journal of Geophysical Research, 116(A05222), doi: 10.1029/2010JA016221.

Kotova, A., E. Roussos, N. Krupp, I. Dandouras, (2015), Modeling of the energetic ion observations in the vicinity of Rhea and Dione, Icarus, 258:402.

Krimigis, S. M., R. B. Decker, E. C. Roelof, M. E. Hill, T. P. Armstrong, G. Gloeckler, D. C. Hamilton, L. J. Lanzerotti, (2013), Search for the exit: Voyager 1 at heliosphere's border with the galaxy, Science, 341(6142):144–147.

Krimigis, S. M., (2011), Saturn's magnetosphere: An example of dynamic planetary systems, American Institute of Physics Conference Proceedings, 1320:213–220, doi: 10.1063/1.3544327.

Krimigis, S. M., E. C. Roelof, R. B. Decker, M. E. Hill, (2011), Zero outward flow velocity for plasma in a heliosheath transition layer, Nature, 474:359–361.

Krimigis, S. M., D. G. Mitchell, E. C. Roelof, R. B. Decker (2010), ENA (E > 5 keV) images from Cassini and Voyager "ground truth": Suprathermal pressure in the heliosheath, American Institute of Physics Conference Proceedings, 1302:79–85, doi: 10.1063/1.3529994.

Krimigis, S. M., et al., (2009a), Analysis of a sequence of energetic ion and magnetic field events upstream from the Saturnian magnetosphere, Planetary and Space Science, 57(14–15):1785–1794, doi: 10.1016/j.pss.2009.02.013.

Krimigis, S. M., D. G. Mitchell, E. C. Roelof, K. C. Hsieh, D. J. McComas, (2009b), Imaging the interaction of the heliosphere with the interstellar medium from Saturn with Cassini, Science, 326:971–973.

Krimigis, S. M., N. Sergis, D. G. Mitchell, N. Krupp, (2007), A dynamic, rotating ring current around Saturn, Nature, 450:1050–1053.

Krimigis, S. M., et al., (2005), Dynamics of Saturn's magnetosphere from MIMI during Cassini's orbital insertion, Science, 307:1270–1273.

Krimigis, S. M., et al., (2004), Magnetosphere imaging instrument (MIMI) on the Cassini mission to Saturn/Titan, Space Science Reviews, 114:233–329.

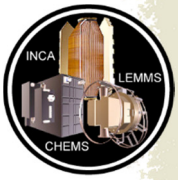

Krimigis, S. M., et al., (2002), A nebula of gases from Io surrounding Jupiter, Nature, 415:994–996.

Krupp, N., et al., (2018a), Energetic electron measurements near Enceladus by Cassini during 2005-2015, Icarus, 306:256–274.

Krupp, N., et al., (2018b), Energetic neutral and charged particle measurements in the inner Saturnian magnetosphere during the Grand Finale orbits of Cassini 2016/2017, Geophysical Research Letters, 45:10,847–10,854, doi: 10.1029/2018GL078096.

Krupp, N., (2016), 12-Energetic-particle environments in the solar system, in Heliophysics: Active stars, their astrospheres, and impacts on planetary environments, (eds.) C. J. Schrijver, F. Bagenal, J. J. Sojka, Cambridge University Press.

Krupp, N., P. Kollmann, M. F. Thomsen, D. G. Mitchell, X. Jia, A. Masters, P. Zarka, (2016a), Global configuration and seasonal variations of Saturn's magnetosphere, in Saturn in the 21st Century, (eds.) K. H. Baines, F. M. Flasar, N. Krupp, Cambridge University Press.

Krupp, N., E. Roussos, C. Paranicas, A. Sicard, G. Hospodarsky, Y. Shprits, (2016b), Energetic particles and waves in the outer planet radiation belts, in Waves, Particles, and Storms in Geospace: A complex Interplay, pp. 373–410.

Krupp, N., (2015), Comparison of plasma sources in solar system magnetospheres, Space Science Reviews, 192:285–295.

Krupp, N., E. Kronberg, A. Radioti, (2015), Jupiter's magnetotail, in Magnetotails in the Solar System, (eds.) A. Keiling, C. M. Jackman, P. A. Delamere, Geophysical Monograph Series, 207, American Geophysical Union, John Wiley & Sons, pp. 85–98.

Krupp, N., (2014), Giant magnetospheres in our solar system: Jupiter and Saturn compared, The Astronomy and Astrophysics Review, 22:75, s00159-014-0075-x.

Krupp, N., et al., (2013), Energetic particle measurements in the vicinity of Dione during the three Cassini encounters 2005-2011, Icarus, 226:617.

Krupp, N., et al., (2012), The Cassini Enceladus encounters 2005-2010 in the view of energetic electron measurements, Icarus, 18:433–447.

Krupp, N., et al., (2010), Environments in the outer solar system, Space Science Reviews, 153:11–59.

Krupp, N., et al., (2009), Energetic particles in Saturn's magnetosphere during the Cassini nominal mission (July 2004 -- July 2008), Planetary and Space Science, 57(14–15):1754–1768, doi10.1016/j.pss.2009.06.010.

Krupp, N., et al., (2005), The Saturnian plasma sheet as revealed by energetic particle measurements, Geophysical Research Letters, 32, 2005GL022829.

Krupp, N., (2005), Energetic particles in the magnetosphere of Saturn and a comparison with Jupiter, Space Science Reviews, 116:345–369.

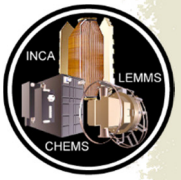

Krupp, N., et al., (2004), Energetic particle observations in the vicinity of Jupiter: Cassini MIMI/LEMMS results, Journal of Geophysical Research, 109, doi: 10.1029/2003JA010111.

Krupp, N., et al., (2002), Leakage of energetic particles from Jupiter's dusk magnetosphere: Dual spacecraft observations, Geophysical Research Letters, 29, doi: 10.1029/2001GL014290.

Kurth, W. S., et al., (2009), Auroral processes, in Saturn from Cassini-Huygens, (eds.) M. K. Dougherty, L. W. Esposito, S. M. Krimigis, Springer, Dordrecht, pp. 333–374.

Lagg, A., N. Krupp, S. Livi, J. Woch, S. Krimigis, M. Dougherty, (2001), Energetic particle measurements during the Earth swing-by of the Cassini spacecraft in August, 1999, Journal of Geophysical Research, 106:30,209–30,222.

Lamy, L., et al., (2013), Multispectral simultaneous diagnosis of Saturn's aurorae throughout a planetary rotation, Journal of Geophysical Research: Space Physics, 118:4817.

Lario, D., S. Livi, E. C. Roelof, R. B. Decker, S. M. Krimigis, M. K. Dougherty, (2004), Heliospheric energetic particle observations by the Cassini spacecraft: Correlation with 1 AU observations, Journal of Geophysical Research, 109(A09S02).

Lebreton, J. P., et al., (2004), High ambitions for an outstanding planetary mission: Cassini-Huygens, European Space Agency Bulletin, 120.

Lewis, G. R., et al., (2010), The calibration of the Cassini-Huygens electron spectometer, Planetary and Space Science, 58:427–436.

Martens, H. R., D. B. Reisenfeld, J. D. Williams, R. E. Johnson, H. T. Smith, (2008), Observations of molecular oxygen ions in Saturn's inner magnetosphere, Geophysical Research Letters, 35(L20103).

Masters, A., et al., (2017), An in-situ comparison of electron acceleration at collionless shocks under differing upstream magnetic field orientations, The Astrophysical Journal, 843:147.

Masters, A., A. H. Sulaiman, N. Sergis, L. Stawarz, A. J. Coates, M. K. Dougherty (2016), Suprathermal electrons at Saturn's bow shock, The Astrophysical Journal, 826:48.

Masters, A., et al., (2013), Electron acceleration to relativistic energies at a strong quasi-parallel shock wave, Nature Physics, 9:164–167.

Masters, A., et al., (2012), The importance of plasma beta conditions for magnetic reconnection at Saturn's magnetopause, Geophysical Research Letters, 39(L08103).

Masters, A., D. G. Mitchell, A. J. Coates, M. K. Dougherty, (2011), Saturn's low-latitude boundary layer 1: Properties and variability, Journal of Geophysical Research, 116(A06210).

Masters, A., et al., (2010), Cassini observations of a Kelvin-Helmholtz vortex in Saturn's outer magnetosphere, Journal of Geophysical Research, 115(A07225), doi: 10.1029/2010JA015351.

Mauk, B. H., (2014), Comparative investigation of the energetic ion spectra comprising the magnetospheric ring currents of the solar system, Journal of Geophysical Research, 119:9729–9746.

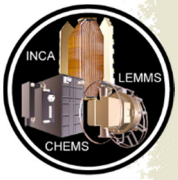

Mauk, B. H., (2012), Radiation belts of the solar system and universe, in Dynamics of the Earth's radiation belts and inner magnetosphere, Geophysical Monograph Series, 199, (eds.) D. Summers, I. R. Mann, D. Baker, M. Schulz, American Geophysical Union, Washington, DC, pp. 405–414.

Mauk, B., F. Bagenal, (2012), Comparative auroral physics: Earth and other planets, in Auroral Phenomenology and Magnetospheric Process, Geophysical Monograph Series, 197, (eds.) A. Keiling et al., American Geophysical Union, Washington, DC, pp. 3–26.

Mauk, B. H., N. J. Fox, (2010), Electron radiation belts of the solar system, Journal of Geophysical Research, 115, A12, doi: 10.1029/2010JA015660

Mauk, B. H., et al. (2009), Fundamental plasma processes in Saturn's magnetosphere, in Saturn from Cassini-Huygens, (eds.) M. K. Dougherty, L. W. Esposito, S. M. Krimigis, Springer, Dordrecht, pp. 281–331.

Mauk, B. H., et al., (2005), Energetic particle injections in Saturn's magnetosphere, Geophysical Research Letters, 32, 2005GL022485.

Mauk, B. H., et al., (2004), Energetic ion characteristics and neutral gas interactions in Jupiter's magnetosphere, Journal of Geophysical Research, 109(A09S12), doi: 10.1029/2003JA010270.

Mauk, B. H., D. G. Mitchell, S. M. Krimigis, E. C. Roelof, C. P. Paranicas, (2003), Energetic neutral atoms from a trans-Europa gas torus at Jupiter, Nature, 421:920–922.

Mauk, B. H., et al., (1999), Storm-like dynamics of Jupiter's inner and middle magnetosphere, Journal of Geophysical Research, 104:22,759-22,778.

Mauk, B. H., S. M. Krimigis, D. G. Mitchell, E. C. Roelof, (1998a), Energetic neutral atom imaging of Jupiter's magnetosphere using the Cassini MIMI instrument, Advances in Space Research, 21:1483–1486.

Mauk, B. H., S. M. Krimigis, D. G. Mitchell, E. C. Roelof, J. Dandouras (1998b), Imaging Saturn's dust rings using energetic neutral atoms, Planetary and Space Science, 46:1349–1362.

McComas, D. J., et al., (2017), Seven years of imaging the global heliosphere with IBEX, Astrophysical Journal Supplement, 229.

McComas, D. J., et al., (2009), Global observations of the interstellar interaction from the Interstellar Boundary Explorer (IBEX), Science, 326, 959.

Menietti, J. D., P. H. Yoon, S. Y. Ye, B. Cecconi, A. M. Rymer, (2010), Source mechanism of Saturn narrowband emission, Annales Geophysicae, 28:1013–1021.

Menietti, J. D., S. -Y. Ye, P. H. Yoon, O. Santolik, A. M. Rymer, D. A. Gurnett, A. J. Coates, (2009), Analysis of narrowband emission observed in the Saturn magnetosphere, Journal of Geophysical Research, 114(A06206).

Menietti, J. D., O. Santolik, A. M. Rymer, G. B. Hospodarsky, A. M. Persoon, D. A. Gurnett, A. J. Coates, D. T. Young, (2008), Analysis of plasma waves observed within local plasma

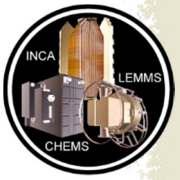

injections seen in Saturn's magnetosphere, Journal of Geophysical Research, 113(A05213), doi: 10.1029/2007JA012856.

Mitchell, D. G., M. E. Perry, D. C. Hamilton, J. H. Westlake, P. Kollmann, H. T. Smith, J. F. Carbary, J. H. Waite Jr., R. Perryman, H. -W. Hsu, J. -E. Wahlund, M. W. Morooka, L. Z. Hadid, A. M. Persoon, W. S. Kurth, (2018), Dust grains fall from Saturn's D-ring into its equatorial upper atmosphere, Science, 362(6410), doi: 10.1126/science.aat2236

Mitchell, D. G., et al., (2016), Recurrent pulsations in Saturn's high latitude magnetosphere, Icarus, 263:94–100.

Mitchell, D. G., et al., (2015), Injection, interchange, and reconnection: Energetic particle observations in Saturn's magnetosphere, in Magnetotails in the Solar System, (eds.) A. Keiling, C. M. Jackman, P. A. Delamere, Geophysical Monograph Series, 207, American Geophysical Union, John Wiley & Sons, pp. 327–344.

Mitchell, D. G., J. F. Carbary, S. W. H. Cowley, T. W. Hill, P. Zarka, (2009a), The dynamics of Saturn's magnetosphere, in Saturn from Cassini-Huygens, (eds.) M. K. Dougherty, L. W. Esposito, S. M. Krimigis, Springer, Dordrecht, pp. 257–279.

Mitchell, D. G., et al., (2009b), Recurrent energization of plasma in the midnight-to-dawn quadrant of Saturn's magnetosphere, and its relationship to auroral UV and radio emissions, Planetary and Space Science, 57(14–15):1732–1742, doi: 10.1016/j.pss.2009.04.002.

Mitchell, D. G., et al., (2009c), Ion conics and electron beams associated with auroral processes at Saturn, Journal of Geophysical Research, 114(A02212), doi: 10.1029/2008JA013621.

Mitchell, D. G., et al., (2005a), Energetic neutral atom emissions from Titan interactions with Saturn's magnetosphere, Science, 308:989–992.

Mitchell, D. G., et al., (2005b), Energetic ion acceleration in Saturn's magnetotail: Substorms on Saturn, Geophysical Research Letters, 32, 2005GL022647.

Mitchell, D. G., C. Paranicas, B. H. Mauk, E. C. Roelof, S. M. Krimigis, (2004), Energetic neutral atoms from Jupiter measured with the Cassini Magnetospheric Imaging Instrument: Time dependence and composition, Journal of Geophysical Research, 109, 2003JA010120.

Mueller, A. L., J. Saur, N. Krupp, E. Roussos, B. H. Mauk, A. M. Rymer, D. G. Mitchell, S. M. Krimigis, (2010), Azimuthal plasma flows in the Kronian magnetosphere, Journal of Geophysical Research, 115(A08203), doi: 10.1029/2009JA015122.

Nordheim, T. A., K. P. Hand, C. Paranicas, C. J. A. Howett, A. R. Hendrix, G. H. Jones, A. J. Coates, (2017), The near surface electron radiation environment of Saturn's moon Mimas, Icarus, 286:56–68.

Nordheim, T. A., et al., (2014), Detection of a strongly negative surface potential at Saturn's moon Hyperion, Geophysical Research Letters, 41:7011–7018.

Ogasawara, K., S. A. Livi, D. G. Mitchell, T. P. Armstrong, N. Krupp, (2011), Properties of energetic particle bursts at dawnside magnetosheath: Cassini observations during the 1999 swing-by, Journal of Geophysical Research, 116(A12207).

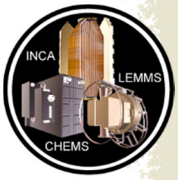

Opher, M., J. F. Drake, B. Zieger, T. I. Gombosi, (2015), Magnetized jets driven by the Sun: The structure of the heliosphere revisited, The Astrophysical Journal of Letters, 800(7).

Orton, G. S., et al., (2009), Review of knowledge prior to the Cassini-Huygens missions and concurrent research, in Saturn from Cassini-Huygens, (eds.) M. K. Dougherty, L. W. Esposito, S. M. Krimigis, pp. 9–54, Springer, Dordrecht.

Palmaerts, B., E. Roussos, N. Krupp, W. S. Kurth, D. G. Mitchell, J. N. Yates, (2016a), Statistical analysis and multi-instrument overview of the quasi-periodic 1-hour pulsations in Saturn's magnetosphere, Icarus, 271:1–18.

Palmaerts, B., A. Radioti, E. Roussos, D. Grodent, J.-C. Gérard, N. Krupp, D. G. Mitchell, (2016b), Pulsations of the polar cusp aurora at Saturn, Journal of Geophysical Research, Space Physics, 121:11,952–11,963, doi: 10.1002/2016JA023497.

Paranicas, C., et al., (2018), Magnetospheric considerations for solar system ice state, Icarus, 302:560–564.

Paranicas, C., et al., (2016), Effects of radial motion on interchange injections at Saturn, Icarus, 264:342–351.

Paranicas, C., et al., (2014), The lens feature on the inner Saturnian satellites, Icarus, 234:155.

Paranicas, C., et al., (2012), Energetic charged particle weathering of Saturn's inner satellites, Planetary and Space Science, 61:60–65.

Paranicas, C., et al., (2010a), Asymmetries in Saturn's radiation belts, Journal of Geophysical Research, 115(A07216), doi: 10.1029/2009JA014971.

Paranicas, C., et al., (2010b), Transport of energetic electrons into Saturn's inner magnetosphere, Journal of Geophysical Research, 115(A09214), doi: 10.1029/2010JA015853.

Paranicas, C., et al., (2008), Sources and losses of energetic protons in Saturn's magnetosphere, Icarus, 197:519–525.

Paranicas, C., et al., (2007), Energetic electrons injected into Saturn's neutral gas cloud, Geophysical Research Letters, 34, 2006GL028676.

Paranicas, C., et al., (2005a), Evidence of Enceladus and Tethys microsignatures, Geophysical Research Letters, 32, 2005GL024072.

Paranicas, C., et al., (2005b), Periodic intensity variations in global ENA images of Saturn, Geophysical Research Letters, 32, 2005GL023656.

Paranicas, C., R. W. Carlson, R. E. Johnson, (2001), Electron bombardment of Europa, Geophysical Research Letters, 28:673.

Parker, E. N., (1961), The stellar-wind regions, The Astrophysical Journal, 134.

Parker, E. N., (1958), Dynamics of the interplanetary gas and magnetic fields, The Astrophysical Journal, 128.

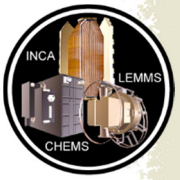

Perry, M. E., et al., (2010), Cassini INMS observations of neutral molecules in Saturn's E-ring, Journal of Geophysical Research, 115(A10206).

Pilkington, N. M., et al., (2015a), Asymmetries observed in Saturn's magnetopause geometry, Geophysical Research Letters, 42:6890–6898.

Pilkington, N. M., et al., (2015b), Internally driven large-scale changes in the size of Saturn's magnetosphere, Journal of Geophysical Research: Space Physics, 120:7289–7306.

Pilkington, N. M., N. Achilleos, C. S. Arridge, A. Masters, N. Sergis, A. J. Coates, M. K. Dougherty, (2014), Polar confinement of Saturn's magnetosphere revealed by in situ Cassini observations, Journal of Geophysical Research: Space Physics, 119:2858–2875.

Pisa, D., G. B. Hospodarsky, W. S. Kurth, O. Santolik, J. Soucek, D. A. Gurnett, A. Masters, M. E. Hill, (2015), Statistics of Langmuir wave amplitudes observed inside Saturn's foreshock by the Cassini spacecraft, Journal of Geophysical Research, 120:2531–2542.

Pryor, W. R., A. Rymer, et al., (2011), The auroral footprint of Enceladus on Saturn, Nature, 472(7343):331–333.

Radioti, A., et al., (2016), A multi-scale magnetotail reconnection event at Saturn and associated flows: Cassini/UVIS observations, Icarus, 263:75–82.

Radioti, A., et al., (2013), Signatures of magnetospheric injections in Saturn's aurora, Journal of Geophysical Research, 118:1922.

Radioti, A., et al., (2009), Transient auroral features at Saturn: Signatures of energetic particle injections in the magnetosphere, Journal of Geophysical Research, 114(A03210), doi: 10.1029/2008JA013632.

Ramer, K. M., M. G. Kivelson, N. Sergis, K. K. Khurana, X. Jia, (2016), Spinning, breathing, and flapping: Periodicities in Saturn's middle magnetosphere, Journal of Geophysical Research: Space Physics, 122:393–416, doi: 10.1002/2016JA023126.

Regoli, L. H., et al., (2018), Statistical study of the energetic proton environment at Titan's orbit from the Cassini spacecraft, Journal of Geophysical Research: Space Physics 123(6):4820–4834.

Regoli, L. H., E. Roussos, M. Feyerabend, G. H. Jones, N. Krupp, A. J. Coates, S. Simon, U. Motschmann, M. K. Dougherty, (2016a), Access of energetic particles to Titan's exobase: A study of Cassini's T9 flyby, Planetary and Space Science, 130:40–53.

Regoli, L. H., A. J. Coates, M. F. Thomsen, G. H. Jones, E. Roussos, J. H. Waite, N. Krupp, G. Cox, (2016b), Survey of pickup ion signatures in the vicinity of Titan using CAPS/IMS, Journal of Geophysical Research: Space Physics, 121, doi: 10.1002/2016JA022617.

Roelof, E. C., (2015), The group abundance fraction: A statistically robust measure of particle composition and of spatial structure in images, Journal of Physics: Conference Series, 577(1):012026.

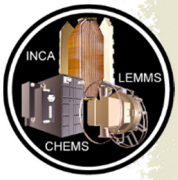

Roelof, E. C., S. M. Krimigis, D. G. Mitchell, R. B. Decker, K. Dialynas, (2012), Cassini ENA images of the heliosheath and Voyager “ground truth”: Thickness of the heliosheath, 10th Anniversary International Astrophysics Conference, American Institute of Physics Conference Proceedings, 1436:265–272.

Roelof, E. C., et al., (2010), Implications of generalized Rankine-Hugoniot conditions for the PUI population at the Voyager 2 termination shock, American Institute of Physics Conference Proceedings, 1302:133–141, doi: 10.1063/1.3529960.

Roussos, E., et al., (2019a), Sources, sinks and transport of energetic electrons near Saturn's main rings, Geophysical Research Letters, 46, doi: 10.1029/2018GL078097.

Roussos, E., et al., (2019b), Jovian cosmic-ray protons in the heliosphere: Constraints by Cassini observations, The Astrophysical Journal, 871:223.

Roussos, E., et al., (2018a), A radiation belt of energetic protons located between Saturn and its rings, Science, 362(6410), doi: 10.1126/science.aat1962.

Roussos, E., et al., (2018b), Heliospheric conditions at Saturn during Cassini's ring-grazing and proximal orbits, Geophysical Research Letters, 45:10,812–10,818, doi: 10.1029/2018GL078093.

Roussos, E., et al., (2018c), Solar energetic particles (SEP) and galactic cosmic rays (GCR) as tracers of solar wind conditions near Saturn: Event lists and applications, Icarus, 300:47–71.

Roussos, E., et al., (2018d), Drift-resonant, relativistic electron acceleration at the outer planets: Insights from the response of Saturn’s radiation belts to magnetospheric storms, Icarus, 305:160–173.

Roussos, E., et al., (2016a), Evidence for dust-driven, radial plasma transport in Saturn’s inner radiation belts, Icarus, 274:272–283.

Roussos, E., et al., (2016b), Quasi-periodic injections of relativistic electrons in Saturn’s outer magnetosphere, Icarus, 263:101–116.

Roussos, E., N. Krupp, C. Paranicas, J. F. Carbary, P. Kollmann, S. M. Krimigis, D. G. Mitchell, (2014), The variable extension of Saturn’s electron radiation belts, Planetary and Space Science, 104(3).

Roussos, E., M. Andriopoulou, N. Krupp, A. Kotova, C. Paranicas, S. M. Krimigis, D. G. Mitchell, (2013), Numerical simulation of energetic electron microsignature drifts at Saturn: Methods and applications, Icarus, 226:1595.

Roussos, E., et al., (2012), Energetic electron observations of Rhea’s magnetospheric interaction, Icarus, 221:116–134.

Roussos, E., et al., (2011), Long- and short-term variability of Saturn’s ionic radiation belts, Journal of Geophysical Research, 116(A02217), doi: 10.1029/2010JA015954.

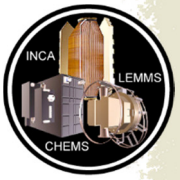

Roussos, E., et al., (2010a), Energetic electron microsignatures as tracers of radial flows and dynamics in Saturn's innermost magnetosphere, Journal of Geophysical Research, 115(A03202), doi: 10.1029/2009JA014808.

Roussos, E., N. Krupp, H. Kruger, G. H. Jones, (2010b), Surface charging of Saturn's plasma absorbing moons, Journal of Geophysical Research, 115(A08225), doi: 10.1029/2010JA015525.

Roussos, E., et al., (2008a), Discovery of a transient radiation belt at Saturn, Geophysical Research Letters, 35, doi: 10.1029/2008GL035767.

Roussos, E., et al., (2008b), Plasma and fields in the wake of Rhea: 3-D hybrid simulation and comparison with Cassini data, Annales Geophysicae, 26:619–637.

Roussos, E., et al., (2008c), Energetic electron signatures of Saturn's smaller moons: Evidence of an arc of material at Methone, Icarus, 193:455–464.

Roussos, E., et al., (2007), Electron microdiffusion in the Saturnian radiation belts: Cassini MIMI/LEMMS observations of energetic electron absorption by the icy moons, Journal of Geophysical Research, 112(A06214), doi: 10.1029/2006JA012027.

Roussos, E., G. H. Jones, N. Krupp, S. M. Krimigis, D. Mitchell, C. Paranicas, (2006), R/2006 S 5, International Astronomical Union Circular, 8773(3).

Roussos, E., et al., (2005), Low energy electron microsignatures at the orbit of Tethys: Cassini MIMI/LEMMS observations, Geophysical Research Letters, 32, 2005GL024084.

Rymer, A. M., D. G. Mitchell, T. W. Hill, E. A. Kronberg, N. Krupp, C. M. Jackman, (2013), Saturn's magnetospheric refresh rate, Geophysical Research Letters, 40:1–5, doi: 10.1002/grl.50530.

Rymer, A. M., (2010), Electron-ion thermal equilibration at Saturn: Electron signatures of ion pick-up, American Institute of Physics Conference Proceedings, 1302:250–255.

Rymer, A., et al., (2009a), Cassini evidence for rapid interchange transport at Saturn, Planetary and Space Science, 57(14–15):1779–1784, doi: 10.1016/j.pss.2009.04.010.

Rymer, A. M., H. T. Smith, A. Wellbrock, A. J. Coates, D. T. Young, (2009b), Discrete classification and electron energy spectra of Titan's varied magnetospheric environment, Geophysical Research Letters, 36(L15109), doi: 10.1029/2009GL039427.

Rymer, A. M., B. H. Mauk, T. W. Hill, C. Paranicas, D. G. Mitchell, A. J. Coates, D. T. Young, (2008), Electron circulation in Saturn's magnetosphere, Journal of Geophysical Research, 113(A01201), doi: 10.1029/2007JA012589.

Rymer, A., et al., (2007), Electron sources in Saturn's magnetosphere, Journal of Geophysical Research, 112(A02201), doi: 10.1029/2006JA012017.

Saur, J., et al., (2006), Anti-planetward auroral electron beams at Saturn, Nature, 439:699–702.

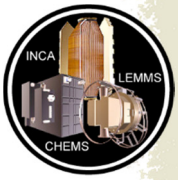

Schenk, P., D. P. Hamilton, R. E. Johnson, W. B. McKinnon, C. Paranicas, J. Schmidt, M. R. Showalter, (2011), Plasma, plumes and rings: Saturn system dynamics as recorded in global color patterns on its midsize satellites, Icarus, 211:740–757.

Schiable, M. J., et al., (2017), High energy electron sintering of icy regoliths: Formation of the PacMan thermal anomalies on the icy Saturnian moons, Icarus, 285:211.

Schippers, P., et al., (2011), Auroral electron distributions within and close to Saturn Kilometric Radiation source region, Journal of Geophysical Research, 116(A05203).

Schippers, P., N. André, R. E. Johnson, M. Blanc, I. Dandouras, A. J. Coates, S. M. Krimigis, D. T. Young, (2009), Identification of photoelectron energy peaks in Saturn’s inner neutral torus, Journal of Geophysical Research, 114(A12212), doi: 10.1029/2009JA014368.

Schippers, P., et al., (2008), Multi-instrument analysis of electron populations in Saturn’s magnetosphere, Journal of Geophysical Research, 113(A07208), 2008JA013098.

Sergis, N., et al., (2018), Mapping Saturn's night side plasma sheet using Cassini's proximal orbit, Geophysical Research Letters, 45:6798–6804, doi: 10.1029/2018GL078141.

Sergis, N., et al., (2017), Radial and local time structure of the Saturnian ring current, revealed by Cassini, Journal of Geophysical Research: Space Physics, 122, doi: 10.1002/2016JA023742.

Sergis, N., et al., (2013), Particle and magnetic field properties of the Saturnian magnetosheath: Presence and upstream escape of hot magnetospheric plasma, Journal of Geophysical Research, 118:1620-1634.

Sergis, N., et al., (2011), Dynamics and seasonal variations in Saturn’s magnetospheric plasma sheet, as measured by Cassini, Journal of Geophysical Research, 116(A04203), doi: 10.1029/2010JA016180.

Sergis, N., et al., (2010), Particle pressure, inertial force, and ring current density profiles in the magnetosphere of Saturn based on Cassini measurements, Geophysical Research Letters, 37, doi: 10.1029/2009GL041920.

Sergis, N., et al., (2009), Energetic particle pressure in Saturn’s magnetosphere measured with the Magnetospheric Imaging Instrument on Cassini, Journal of Geophysical Research, 114(A02214), doi: 10.1029/2008JA013774.

Sergis, N., et al., (2007), Ring current at Saturn: Energetic particle pressure in Saturn’s equatorial magnetosphere measured with Cassini/MIMI, Geophysical Research Letters, 34(L09102), 10.1029/2006GL029223.

Shemansky, D. F., et al., (2009), The Saturn hydrogen plume, Planetary and Space Science, 57:1659–1670.

Simon, S., E. Roussos, C. S. Paty, (2015), The interaction between Saturn’s moons and their plasma environments, Physics Reports, 602:1–65.

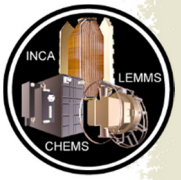

Simon, S., H. Kriegel, J. Saur, A. Wennmacher, F. M. Neubauer, E. Roussos, U. Motschmann, M. K. Dougherty, (2012), Analysis of Cassini magnetic field observations over the poles of Rhea, Journal of Geophysical Research, 117(A07211).

Sittler, E. C., et al., (2009), Energy Deposition Processes in Titan's Upper Atmosphere and Its Induced Magnetosphere, in Titan from Cassini-Huygens, (eds.) R. H. Brown, J. -P. Lebreton, J. H. White, Springer, Dordrecht.

Sittler, E. C., Jr., et al., (2008), Ion and neutral sources and sinks within Saturn's inner magnetosphere: Cassini results, Planetary and Space Science, 56, doi: 10.1016/j.pss.2007.06.006.

Sittler, E. C., et al., (2006), Energetic nitrogen ions within the inner magnetosphere of Saturn, Journal of Geophysical Research, 111(A09223), doi: 10.1029/2004JA010509.

Smith, C. G. A., (2018), Interaction of Saturn’s dual rotation periods, Icarus, 302:330–342, doi: 10.1016/j.icarus.2017.11.016.

Smith, H. T., A. M. Rymer, (2014), An empirical model for the plasma environment along Titan's orbit based on Cassini plasma observations, Journal of Geophysical Research, 119, 2014JA019872.

Smith, H. T., (2010), Neutral clouds and their influence on pick-up ions in Saturn’s magnetosphere, American Institute of Physics Conference Proceedings, 1302:256–262.

Smith, H. T., R. E. Johnson, M. E. Perry, D. G. Mitchell, R. L. McNutt, D. T. Young, (2010), Enceladus plume variability and the neutral gas densities in Saturn’s magnetosphere, Journal of Geophysical Research, 115(A10252), doi: 10.1029/2009JA015184.

Smith, H. T., et al., (2009), Investigation of energetic proton penetration in Titan’s atmosphere using the Cassini INCA instrument, Planetary and Space Science, 57(13):1538–1546, doi: 10.1016/j.pss.2009.03.013.

Smith, H. T., M. Shappirio, R. E. Johnson, D. Reisenfeld, E. C. Sittler, F. J. Crary, D. J. McComas, D. T. Young, (2008), Enceladus: A potential source of ammonia products and molecular nitrogen for Saturn's magnetosphere, Journal of Geophysical Research, 113(A11206), doi: 10.1029/2008JA013352.

Sorba, A.M., N. A. Achilleos, P. Guio, C. S. Arridge, N. M. Pilkington, A. Masters, N. Sergis, A. J. Coates, M. K. Dougherty, (2017), Modeling the compressibility of Saturn's magnetosphere in response to internal and external influences, Journal of Geophysical Research: Space Physics, 122(2):1572–1589.

Stephan, K., et al., (2016), Cassini's geological and compositional view of Tethys, Icarus, 274:1–22, doi: 10.1016/j.icarus.2016.03.002.

Stevens, M. H., J. S. Evans, J. Lumpe, J. H. Westlake, J. M. Ajello, E. T. Bradley, L. W. Esposito, (2015), Molecular nitrogen and methane density retrievals from Cassini UVIS dayglow observations of Titan’s upper atmosphere, Icarus, 247:301.

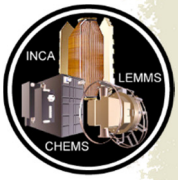

Teolis, B. D., et al., (2010), Cassini finds an oxygen-carbon-dioxide atmosphere at Saturn's icy moon Rhea, Science, 330:1813–1815.

Thomsen, M. F., D. G. Mitchell, X. Jia, C. Jackman, G. Hospodarsky, A. Coates, (2015), Plasmapause formation at Saturn, Journal of Geophysical Research: Space Physics, 120, 2015JA021008.

Thomsen, M. F., et al., (2014), Ion composition in interchange injection events in Saturn's magnetosphere, Journal of Geophysical Research, 119:9761–9772.

Thomsen, M., et al., (2013), Saturn's magnetospheric dynamics, Geophysical Research Letters, 40:5337–5344.

Thomsen, M. F., et al., (2012), Saturn's inner magnetospheric convection pattern: Further evidence, Journal of Geophysical Research, 117(A09208).

Thomsen, M. F., D. B. Reisenfeld, D. M. Delapp, R. L. Tokar, D. T. Young, F. J. Crary, E. C. Sittler, M. A. McGraw, J. D. Williams, (2010), Survey of ion plasma parameters in Saturn's magnetosphere, Journal of Geophysical Research: Space Physics 115:A10.

Tobie, G., et al., (2014), Science goals and mission concept for the future exploration of Titan and Enceladus, Planetary and Space Science, 104:59.

Tobiska, W. K., (2004), SOLAR2000 irradiances for climate change research, aeronomy and space system engineering, Advances in Space Research, 34:1736–1746.

Tokar, R. L., et al., (2008), Cassini detection of water-group pick-up ions in the Enceladus torus, Geophysical Research Letters, 35, doi: 10.1029/2008GL034749.

Westlake, J. H., J. H. Waite, J. M. Bell, R. Perryman, (2014), Observed decline in Titan's thermospheric methane due to solar cycle drivers, Journal of Geophysical Research: Space Physics, 119:8586–8599, doi: 10.1002/2014JA020394.

Westlake, J. H., J. H. Waite, Jr., N. Carrasco, M. Richard, T. Cravens, (2014), The role of ion-molecule reactions in the growth of heavy ions in Titan's ionosphere, Journal of Geophysical Research, 119:5951–5963.

Westlake, J. H., et al., (2012), The observed composition of ions outflowing from Titan, Geophysical Research Letters, 39(L19104).

Westlake, J. H., J. M. Bell, J. H. Waite, Jr., R. E. Johnson, J. G. Luhmann, K. E. Mandt, B. A. Magee, A. M. Rymer, (2011), Titan's thermospheric response to various plasma environments, Journal of Geophysical Research, 116(A03318).

Wulms, V., J. Saur, D. F. Strobel, S. Simon, D. G. Mitchell, (2010), Energetic neutral atoms from Titan: Particle simulations in draped magnetic and electric fields, Journal of Geophysical Research, 115(A06310), doi: 10.1029/2009JA014893.

Yelle, R.V., D. F. Strobel, E. Lellouch, D. Gautier, (1997), Engineering models for Titan's atmosphere, in Huygens: Science, Payload and Mission, pp. 243–256.

- - - - - - - - - - - - - -